Peak glacial-to-Heinrich-1 changes in Denmark Strait Overflow and seawater stratification in the Nordic Seas, a switchboard of changes in Atlantic Meridional Overturning Circulation and the 'Nordic Heat Pump'

Michael Sarnthein[1] and Patrick Blaser[1]

[1]Affiliation not available

April 25, 2024

Peak glacial-to-Heinrich-1 changes in Denmark Strait Overflow and seawater stratification in the Nordic Seas, a switchboard of changes in Atlantic Meridional Overturning Circulation and the 'Nordic Heat Pump'

Michael Sarnthein[1)] and Patrick Blaser[2)]

[1)] Institut für Geowissenschaften, University of Kiel, D-24118 Kiel, Germany

<michael.sarnthein@ifg.uni-kiel.de>

[2)] ISTE, University of Lausanne, CH-1015 Lausanne, Switzerland

<patrick.blaser@unil.ch>

ABSTRACT (246 w.)

Today, the sub-surface Denmark Strait Overflow (DSO) and the Iceland Scotland Overflow form the starting points of Atlantic Meridional Overturning Circulation and compensate for the poleward flowing Norwegian and Irminger branches of the North Atlantic surface current that drive the 'Nordic Heat Pump'. During peak glacial and early deglacial times, ice sheets on Iceland and Greenland, and ice-induced isostatic and eustatic sea-level changes reduced the Denmark Strait aperture and DSO. Nonetheless, extremely high benthic stable carbon and oxygen isotope values together with very high ventilation ages of bottom waters reflect a north-south density gradient of intermediate-waters and persistent flow of partially Arctic-sourced waters through both the Denmark Strait and the Faeroe Channel, similar to today. The first arrival of Heinrich -1 meltwaters northwest of Iceland, arriving from the southwest around 18.4 cal ka, accompanied a tipping point in DSO circulation, documented by reduced ventilation and ventilation ages, a 3°C warming, and increased radiogenic Nd isotope signatures in sediments at luff-side Site PS2644. These records suggest a sudden subsurface incursion of Atlantic intermediate waters across basaltic sediments from S.E. of Iceland. Deep-water convection off Norway then was replaced by weak brine water formation, coeval with a breakdown of the 'Nordic Heat Pump' evidenced by a temperature drop on Greenland. After 16.2 cal. ka, a major meltwater outbreak from the Barents ice shelf led to modified Heinrich-1-style circulation until ˜15.1 cal ka. Vice-versa, the DSO intensified during interstadial and Holocene times, then causing sediment hiatuses at site PS2644.

KEY WORDS:

Nordic Seas, Deep-water formation, Denmark Strait Overflow, Age control of Heinrich stadial 1, Nordic Heat Pump, Atlantic Meridional Overturning Circulation

KEY POINTS:

The Overflow of Nordic Sea's deep waters forms the onset of Atlantic Meridional Overturning Circulation being enhanced at interstadial times

Sediments off N. Iceland show a joint onset of deglacial meltwater dilution and 3-degree warming of the Denmark Strait Overflow 18400 yr ago

Deglacial changes in circulation caused Heinrich Stadial 1, a temporary end of heat advection to European high latitudes 18400–15000 yr ago

PLAIN LANGUAGE SUMMARY (200 w.)

Differences in salt content of North Atlantic surface waters drive variations in Nordic Seas' overturning circulation. These form a switchboard for changes in the oceanic heat transport to North European high latitudes, the 'Nordic Heat Pump', and for Atlantic Meridional Overturning Circulation (AMOC). We deduced changes in the Nordic Seas' overturning circulation during the peak last glacial and early deglacial from two high-resolution marine sediment cores with centennial-scale age resolution based on the technique of radiocarbon plateau tuning (22-15 cal. ka). Sediment data suggest that the salinity of surface water, advected from the North Atlantic, started to drop about 18 400 years ago. This drop accompanied a 3°C rise in temperature and a drop in ventilation and radiocarbon ventilation age of Denmark Strait Overflow waters feeding the AMOC. Also, it paralleled a massive rise in the radiocarbon reservoir age of surface waters up to 2000 yr and an abrupt breakdown of Nordic Seas' deep-water convection off Norway. Accordingly, Atlantic waters were replaced by less saline polar waters, marking a breakdown of the Nordic Heat Pump and start of 'Heinrich Stadial 1' as reflected by a coeval cooling documented on top of the Greenland ice sheet, lasting until ˜15.1 cal. ka.

INTRODUCTION

The Denmark Strait Overflow (DSO; Fig. 1) with its exceptionally high density plays a key role for ˜50% of the Atlantic meridional overturning circulation (AMOC) and thereby, for global deep-ocean circulation. The DSO is closely associated with the "Nordic Heat Pump", and any changes therefore have major implications for northern hemispheric climate, moreover, it is crucial for deep-ocean ventilation and radiocarbon uptake. Today, the flux of DSO is long-term fairly stable with >3 Sv entering from the southern Greenland Sea and Arctic Ocean (Brakstad et al., 2023). Further 5 Sv are entrained into DSO during its overflow in the Irminger Sea to the south of the Denmark Strait, where a 2.5 km deep descend acts in stabilizing the DSO (data of Biastoch et al., 2003 and 2021; Kösters, 2004, Kösters et al., 2005; Kaese & Oschlies, 2000, Kaese et al. 2003 and refs. therein)

East of Faroe the DSO is paralleled by the Iceland-Scotland Overflow Water (ISO), also enfolding ˜1.4–2.4 Sv, being supplied to the N.E. North Atlantic and subsequently, after having passed the Charlie Gibbs Fracture Zone, into the AMOC in the western Atlantic (Hansen et al., 2000; Sessford et al., 2019; Biastoch et al., 2021).

Important characteristics of modern DSO waters are low bottom water temperatures near -1°C, high bottom water salinities of 34.9 psu, and densities (σ) of 27.8-28.05 kg/m^3 for Theta=2°C at the bottle neck of the Denmark Strait (Whitehead et al., 1974; Macrander and Käse, 2007; Haine, 2021). A slight but persistent north-south density gradient is indicated for the Last Glacial Maximum (LGM, 19–23 thousand calibrated yr before present; cal. ka) by δ^{18}O records of single specimens of epibenthic foraminifera (Millo et al., 2006) and confirmed by the distribution pattern of ε_{Nd} isotopes, a tracer of dominantly continental or basaltic sediments overflown by bottom waters (Larkin et al., 2022; Blaser et al., 2020).

To monitor short-term variations in the DSO over peak glacial-to-early deglacial climate change (22 - 15 cal. ka; here 'ka' is used for 'kilo yr ago' in the sense of BP = Before Present = 1950 yr AD) we now employ, partly refine, and supplement published centennial-scale proxy records obtained from sediment Core PS2644, a site that marks the southern margin of the Blosseville Basin, that is the northern funnel to the Denmark Strait north of westernmost Iceland (Fig. 1; Voelker, 1999; Millo et al., 2006). We compare the effect and origin of long-term climate trends and intermittent short, centennial-to-millennial-scale episodes of major

cold spells with episodes of fast climate warming, regimes in part lasting until today. The very last major Greenland stadial we redefined as Heinrich Stadial 1a and b (HS-1a and b), in contrast to a redefinition of stadials proposed by Andrews and Voelker (2018). On the basis of advanced age control (details are given below) our definition of HS-1 differs strongly from that previously given by Hodell et al. (2017) based on sediments from the southern subpolar North Atlantic.

Moreover, we compare our records with proxy data and circulation models of stadial and interstadial analogue variations over Marine Isotope Stage 3 (MIS3) near to the northern entrance of the Denmark Strait as proposed by Hagen and Hald (2002), Sadatzki et al. (2020), and Sessford et al. (2018, 2019). The latter authors report on distinct changes in MIS3 bottom water temperature, which we now try to reproduce for late MIS2. Sessford et al. (2019) proposed pathways of brine water-induced intermediate waters that finally might have been funneled into the DSO, assuming a water column homogenous in the Nordic Seas down to 1500 m.

We test this model by means of a number of multiproxy records from Site PS2644, compared to pertinent records obtained from outside on the basis of centennial-scale age resolution (Sarnthein et al., 2020): (i) We employ records from two neighbor sites at the western margin of the Vøring Plateau in the eastern Nordic Seas (Fig. 1; GIK23074 and MD95-211), where brine water formation is widely accepted to have occurred during HS-1 (Meland et al., 2008; Waelbroeck et al., 2011). (ii) We compare coeval paleoceanographic records obtained south of Iceland in the northern North Atlantic (Thornalley et al., 2011; Millo et al., 2006; Sarnthein et al., 1994).

In this way we focus on minor and major changes in the origin of early deglacial DSO waters and related changes in the flow geometry of the eastern Nordic Seas and of North Atlantic intermediate- and deep-water circulation. Changes in flow geometry were possibly linked to crucial tipping points in the composition of DSO waters, items to be constrained in this study. The origin of these changes appears highly important for a better understanding of past and future trends of the "Nordic Heat Pump" and European climate change (*sensu* Jansen et al., 2020; Ditlevsen and Ditlevsen, 2023).

OCEANOGRAPHIC WATCHDOG POSITIONS of SITES PS2644 AND GIK23074

Bathymetry and modern patterns of surface and bottom water circulation in the Denmark Strait (Fig. 1; today: ~630 m w.d.) are detailed by Kösters et al. (2004). Macrander et al. (2007) present details of the modern DSO structure being ruled by geostrophic forcing. Sediment Core PS2644 lies within the lower portion of the modern plume funneled into the DSO (Käse et al., 2003). Prior to entering the Denmark Strait, Norwegian Sea Deep Water (NSDW) today is entrained from both the Greenland Basin and Arctic Ocean (Brakstad etal., 2023), a scenario to be traced back over last glacial and early deglacial times 22–15 cal. ka.

Sediments of Core PS2644 are well suited to monitor past glacial-to-early deglacial variations in the flow of surface and deep-water masses since the site lies close to the Polar Front, that is the mean position of the border of perennial sea ice, the boundary between the East Iceland Current (EIC) and the nearshore North Iceland Irminger Current (NIIC) (Fig. 1; Voelker, 1999), while not lying too close to the Denmark Strait where extreme winnowing due to strong bottom currents largely prevents any sediment deposition. To achieve an undisturbed and largely continuous sediment record of past changes in the geometry of ocean water masses, Site PS2644 at 777 m water depth on top of a narrow hemipelagic sediment ridge was chosen after careful selection by means of a high-resolution PARASOUND parametric echosounder system (Hubberten et al., 1995). As detailed in Voelker (1999) the site shows a sediment drift free from lateral near-bottom sediment input like sediment slumps and/or turbidity currents (Fig. 2a; Fig. S1).

Core GIK23074 was retrieved from the western margin of the Vøring Plateau right below the North Atlantic Current (NAC), but far away from the Norwegian margin (Fig. 1; Voelker, 1999). The site is marked by exceptionally high, yet undisturbed hemipelagic sedimentation rates (25-60 cm /ky; Fig. 2b), thus providing a unique high-resolution (17-50 yr per cm sediment depth) record of ocean history in the eastern Nordic Seas at 1157 m water depth.

AGE CONTROL and PALEOCEANOGRAPHIC PROXIES

Precise age control of marine sediment records PS2644 and GIK23074 is essential for constraining the objectives of this study. Age control has been based on various conventional, correlation-based age tie points by Voelker (1999) and Voelker et al. (1998 and 2000). Finally, however, we based our age model on the technique of ^{14}C plateau tuning (Figs. 2a and b) (Sarnthein et al., 2020 and 2023). The different approaches are listed below:

* Distinct features in the planktic δ^{18}O records were correlated to apparently analogous age-calibrated δ^{18}O oscillations in ice core records GISP2 and NGRIP, where ages are based on incremental time scales (Grootes and Stuiver, 1997; Svensson et al., 2008) (Fig. S1; Voelker, 1999).

* Likewise, distinct variations in % *Neogloboquadrina pachyderma*sin (Nps; in "old" teminology) served as tracer of short-term SST changes that were used as stratigraphic markers by comparison to temperature variations dated in Greenland ice core records.

* The Vedde volcanic ash layer was used as tracer dated by land plants at ˜10.31±50 yr ^{14}C ka (= 12.1 cal. ka) on the basis of ambient plant macrofossils (age revised by Birks et al., 2017; Bronk Ramsey et al., 2020).

* Initial age control was established by means of a high-resolution suite of planktic ^{14}C ages in Core PS2644, using the general assignment of a hypothetical Marine Reservoir Age (MRA) of 400 yr (Voelker, 1999; Voelker et al., 1998). This assumption, however, has now been subject to major revision (Sarnthein et al., 2015 and 2020) as shown below.

* On top of a simple conventional stratigraphic alignment of planktic^{14}C ages, we further refined the age control by defining local planktic ^{14}C age plateaus and plateau boundaries that were tuned as cal. age tie points to pertinent age-calibrated structures in the atmospheric ^{14}C record of Lake Suigetsu (Table 1; Sarnthein et al., 2023). In turn, Suigetsu age control is based on U/Th-based model ages of Bronk Ramsey et al., 2020 (details of age derivation in Sarnthein et al., 2020 and 2023) (Figs. 2a and b). We are aware that our approach is in conflict with allegations of Bard and Heaton (2021) claiming that the approach is flawed. However, we trust in ^{14}C plateau tuning for various crucial reasons: (i) Different from Bard and Heaton (op. cit.) we have clearly shown that past centennial to millennial-scale fluctuations of the atmospheric ^{14}C record have been authentic (Sarnthein et al. (2023). (ii) Our technique of plateau tuning solely relies on the tuning of a whole suite of ^{14}C plateaus in the atmosphere and a sediment core each (Figs. 2a+b), thus can clearly distinguish and/or exclude potential fake plateaus in a sediment core, such as given for Core GIK23074 for the top portion of HS-1 (Fig. 2b). (iii) Our text (Figs. 4 and 5) is demonstrating two prominent cases of abrupt deglacial climate change during Heinrich stadial 1 at 18.4 and 16.2 cal. ka, where the ^{14}C plateau-based age estimates precisely match pertinent estimates based on the incremental age scale of the North GRIP ice core with less than 100 years deviation, results that are far from incidental and *would not be revealed* by any other stratigraphic method. (iv) On the basis of numerous details, we have refuted one-by-one the allegations of Bard and Heaton (op.cit.), as published in the discussion section of their article (Grootes and Sarnthein, 2021; Sarnthein and Grootes, 2021), though ignored by Bard and Heaton.

Calendar-age uncertainties of the atmospheric ^{14}C plateau boundaries employed for our tuning approach hardly exceed ˜50 to ˜100 yr each. Local MRA of planktic foraminifers and surface waters were derived from the age difference between the average ^{14}C age estimated for paired, that is, coeval atmospheric and marine plateaus based on^{14}C plateau tuning (Sarnthein et al., 2020, and references therein).

* In addition, a single U/Th-based cal. age was obtained from a solitary coral in Core MD95-2011. This age was compared with the^{14}C ages of paired planktic and benthic foraminifera specimens (Fig. 3), thereby largely confirming the paired age estimates and MRA derived on the basis of ^{14}C plateau tuning of the planktic ^{14}C record (unpubl. comm. of Dreger, 2000; thorium/uranium data of Lomitschka and Mangini [1999]. The ratio of thorium to uranium in each sample, which yield the calendar age of the coral, were measured by thermal ionisation mass spectrometry (TIMS) at the Heidelberger Akademie der Wissenschaften (Heidelberg, Germany) according to the method outlined by Bollhofer et al. (1996) and Neff et al. (1999).

* Sedimentation rates with multi-centennial time resolution were derived from the age interpolation of sediment sections using the cal. age of planktic ^{14}C plateau boundaries (Fig. 2a and b). The estimates were widely supported by means of ages independent of^{14}C plateau tuning such as the linear age interpolation between conventional age tie points to pertinent ages of ice core record GISP2 (Voelker, 1999; Fig. S1).

* To a large extent, Site **PS2644 lacks modern and Holocene reference values** for most proxy records employed in this study. Except for a few cm thick ^{14}C-dated sediment layer that forms the actual core top, a strong DSO flow has hindered any Holocene sediment deposition and/or led to sediment erosion prevalent over most of the last ˜15 cal. ka (Voelker, 1999; Kuijpers et al., 2003).

* The derivation and constraints of various paleoceanographic proxy values employed in this study are given in Supplementary Text no. 1.

PS2644: FOUR STRATIGRAPHIC TIME SEGMENTS ˜22–15 cal. ka

The PS2644 sediment section representing LGM and HS-1 times starts and ends with major **stratigraphic gaps** prior to ˜21.9 cal. ka and subsequent to ˜15.1 cal. ka (Fig. 2a). The gaps occur near the end of Greenland Interstadial (GI) 2 and close to the end of HS1, shortly prior to the Bolling-Allerod (B/A) interstadial that is lost by erosion or non-deposition (Fig. S1; Voelker, 1999, and Voelker et al., 2000). This sediment gap is documented by X-ray radiography as distinct unconformity at 54-53 cm composite core depth, right below the Vedde Ash layer, 12.6 cal. ka (*sensu* Voelker, 1999, and Voelker and Haflidason, 2015). The stratigraphic gaps probably result from enhanced sediment winnowing due to the constriction of an enhanced inflow to the Denmark Strait near to its northern entrance.

This peak-glacial-to-early-deglacial sediment record of PS2644 for MIS2 is partitioned into four stratigraphic time segments I through IV that lasted from 21.8–19.8, 19.8–18.4, 18.4–17.2, and 17.2–˜15.1 cal. ka, based on epibenthic ventilation ages, changes in the stable C and O isotope composition of planktic and epibenthic foraminifera (Nps and mainly *Cibicidoides lobatulus*), and less distinct, planktic MRA. The partitioning is also reflected by the ε_{Nd} and Pb isotope records, moreover, by distinct changes in sedimentation rate (Fig. 4). It is important to note that the time segments apply to the suite of structures in the proxy records of both the cores PS2644 near Iceland and GIK23074 from the eastern Nordic Seas.

Time segment (I), 21.8–19.8 cal. ka, in PS22644 covers the top portion of the Last Glacial Maximum (LGM; as defined by Mix et al., 2001), while **time segment (II) 19.8–18.4 cal. ka**already reflects the end of the LGM, as suggested by a first major deglacial rise in eustatic sea level starting at 19.4 cal. ka (based on purely atmospheric ^{14}C ages of Hanebuth et al., 2009). During segments I and II, sea ice-covered subsurface waters of the East Greenland Current (EGC) at PS2644 (Sadatzki et al., 2020) are marked by minimum temperature and peak salinity values as reflected by fairly persistent planktic δ^{18}O values of 4.5 SST of 3.7°C based on census counts of planktic foraminifera species (Pflaumann et al., 2003; Millo et al., 2006). Time segment I shows a maximum MRA near 2200 yr, that slightly dropped to ˜1900 yr after 19.8 cal. ka (Fig. 4).

During time segment I, bottom waters at PS2644 were marked by a bipartite population of epibenthic δ^{13}C values. One of them presents the highest δ^{13}C values and, despite all processes of ocean mixing, the highest deep-water ventilation recorded in the global ocean (Millo et al., 2006; Duplessy et al., 2002), clearly predominant over 21.8–20.3 cal. ka, when bottom water ventilation ages reached up to 2500 ^{14}C yr.

Radiogenic isotopes in the detrital sediment fraction indicate a mixture of Arctic and European sources of the sediment, with a reduced contribution from nearby Iceland (Fig. 4 and 5; Struve et al., 2019; Larkin et al., 2021; Blaser et al., 2020). We hypothesize that this could have been caused by the complete glaciation of Iceland and/or a change in ocean currents shielding the site from Icelandic input. Interestingly, the authigenic sediment fraction exhibited significantly more radiogenic signatures in both Nd and Pb. A similar effect has been observed in front of the Barents Shelf (Struve et al. 2019) and in the eastern subpolar North Atlantic (ODP980; Crocket et al. 2013) and attributed to the glacial erosion of terrestrial metal oxides in Northwest Europe and their supply to the ocean.

During **time segment** II, after 19.8 cal. ka, the antecedent high in bottom water ventilation age was short-term replaced by very low ages of 100-400 yr. North of Iceland they mark an early deglacial incursion of waters reflecting a direct contact with the atmosphere nearby, closely resembling ages that already marked the end of GI 2, and more important, LGM bottom water ages found at Site GIK23074 in the eastern Nordic Seas. Moreover, we find a distinct rise in radiogenic εNd values of the detritus up to -5, which traces an increased contribution by Icelandic basalts passed by DSO waters prior to reaching Site PS2644 (Fig. 4), or increased supply through an early deglaciation of parts of Iceland (*sensu* Crocket et al., 2012).

Time segment III, 18.4–17.2 cal. ka, reflects a phase of transition, when planktic $\delta^{18}O$ values at PS2644 show a marked gradual drop by more than 1.5 per mil (Fig. 4). The drop primarily reflects a drop in sea surface salinity induced by a lateral advection of meltwaters from southwest, from the Irminger Sea, and thus records the onset of HS-1. Also, foraminifera census counts reflect a slight SST rise up to 4°C (Sarnthein et al., 2001). Over this time, local MRA dropped to 1670-1780 yr, a value slightly lower than before, but still reflecting a reduced carbon exchange of sub-surface waters with the atmosphere, impeded by ongoing perennial sea ice cover. At the eastern Site GIK23074 MRAs at the onset of time segment III showed an impressive sudden rise from 1175 yr up to 1900 yr, a level equating that found at the western Site PS2644 (Figs. 2b and 3).

Like surface waters, bottom waters document a major change near 18.4 cal. ka: The maxima of benthic $\delta^{18}O$ values measured on single epibenthic specimens reveal a rapid, centennial-scale^{18}O depletion by 0.8 a rise in bottom water temperature of up to 3.4°C (Fig. 4). At this time, the data population with extremely high epibenthic $\delta^{13}C$ values has disappeared in favor of medium high values, coeval with a renewed short-term reduction of bottom water ventilation ages down to 750 yr near 17.5 cal. ka. Once more, εNd signatures in both the detrital and authigenic fractions have increased, indicating an elevated supply of Icelandic volcanogenic material overflown by DSO waters prior to reaching Site PS2644 (Fig. 4) or delivered to the site directly by surface currents such as the North Iceland Irminger Current (Fig. 1). The contemporaneous authigenic$^{206}Pb/^{204}Pb$ -based ratios show a pronounced short-lasting maximum (Fig. 5), which could result from an increased delivery of Pb glacially eroded from Northwest Europe 18.4-17.0 cal. ka.

Time segment IV, 17.2–15.1 cal. ka (i.e., until the onset of a major hiatus), presents the full maturation of the HS-1 sub-ice meltwater regime as reflected by a persistent minimum in planktic $\delta^{18}O$. Near the very onset, this interval was marked by a short-term SST peak of 7.5°C (census counts of planktic foraminifera species; Fig. 15c of Voelker, 1999). As in antecedent periods, MRA of 1900 years continued. By contrast, paired bottom water ages were as low as 1100 to 1550 ^{14}C years, significantly lower than during the LGM. As in time segment III, epibenthic $\delta^{13}C$ values of bottom water ventilation were modestly high (0.6-1.4

The onset of time segment IV shows a remarkable sudden rise in bulk sedimentation rates at PS2644, almost by a factor of three, with sediments marked by a high in the concentration of ice-rafted hematite-stained quartz grains originating from (North-) East Greenland (Voelker, 1999). At the same time, detrital$^{206}Pb/^{204}Pb$ ratios decreased while εNd became more radiogenic (Fig. 4), which would agree with an increased delivery of Tertiary basalt sediment. On the expense of the "European" source (Fig. 5) the basalt signal then may have come from the nearby Iceland-Scotland Ridge east of Iceland, overflown by the North Iceland Jet, when heading west for Site PS2644. Also, Fig. 5 may suggest an input of basalt debris from major basalt sources in East Greenland south of 70°N. Conversely, however, we regard this east-west sediment transport as unlikely, since it would need to cross the (sea-ice covered) frontal systems of the East Greenland Current flowing toward southwest (Fig. 1).

Altogether, MRAs and bottom water ventilation ages at **Site GIK23074** (Fig. 3) reveal a suite of changes in differential stratification of the eastern Nordic Seas contemporary with that in the west, at PS2644 (Fig. 1). In addition, however, time segment IV has been dissected near 16.15 cal. ka by a subsequent major drop in both MRA and bottom water ventilation age (Fig. 2b and 3). The drops are tied to the great late-deglacial meltwater outbreak from the Barents Shelf as documented by a short-term extreme low in planktic $\delta^{18}O$ values extending south to the Faeroe Isles (Weinelt et al, 1991; Voelker, 1999).

DISCUSSION – LINKAGES BETWEEN CHANGING SOURCES OF DSO WATERS AND SHORT-TERM CHANGES IN SEA SURFACE SALINITY AND CLIMATE

In search of differential sources of DSO waters

Today, DSO source waters are intermediate and deep waters of the Icelandic and Greenland Seas, that means, convection-induced waters of North Atlantic sources (NAC), Arctic Ocean waters, and the subsurface North Iceland Jet (NIJ) (Fig. 1). The isotope composition and ventilation age of waters feeding the DSO as recorded at Site PS2644 (and by fragmentary records from the southern exit of the Denmark Strait; Millo et al., 2006) document a number of short-term millennial-scale changes in circulation geometry (Fig. 4) to be compared with the modern regime of the overflow. Differential ventilation ages suggest a distinction of three different modes of DSO water: (1) Extremely low ages mark the DSO mode 1, both at the very end of GI 2 at 21.8 cal. ka (GICC05 record of Wolff et al., 2010) and at the end of the LGM between ˜19.5 and 18.7 cal. ka (Mix et al., 2001), the center of time segment II (Fig. 4). (2) Most of LGM time segment I displays DSO mode 2 marked by a stable high ventilation age of 2200-2500 years, almost recurring near 18.7–18.4 cal. ka. (3) Finally, time segments III and IV show DSO mode 3 with an intermediate ventilation age of 1100-1600 years. Near 17.6–17.3 cal. ka, mode 3 starts with an age minimum of ˜700-960 years similar to DSO mode 1. Finally, this mode continued until about 15.1 cal. ka (Fig. 2a), the base of a sedimentation gap (Voelker 1999).

DSO modes 1 and 2 are paired with two separate, but coeval populations of epibenthic $\delta^{13}C$ values measured on single foraminifera specimens in each sediment sample, one with 0.8–1.4 with 1.4–1.7 estimates of global ocean ventilation (Millo et al., 2006). In part, these extreme populations may just represent the product of seasonal to decadal variability. The highest values suggest that DSO mode-2 waters then have been entrained from polar regions (Brakstad et al., 2023; in harmony with a model of Haine, 2021) that are largely bare of any organic carbon production. Based on data of single foraminifera specimens, maximum $\delta^{18}O$ values of 5.5 record extremely low intermediate-water temperatures typical of an Arctic source (Waelbroeck et al., 2011). Conversely, briefly intercalated ventilation age minima of DSO mode 1 indicate that a major portion of these waters then may have originated nearby, likely from convection in the eastern Nordic Seas, near Site GIK23074, as discussed below (Fig. 3).

Nd and Pb radiogenic isotope signatures suggest the sediment related to DSO modes 1 and 2 was largely sourced from northern Europe, Iceland, and probably, basaltic sediments on the Iceland-Scotland Ridge overflown by the North Iceland Jet (Figs. 1, 4, and 5). Altogether, DSO modes 1 and 2 may have come close to patterns of modern circulation geometry. The flow strength of mode 2, however, was probably reduced as suggested by medium high sedimentation rates at PS2644 (Fig. 4). Conversely, the flow of mode 1 was probably much stronger. At >21.8 cal. ka, it resulted in a sedimentation gap and erosional hiatus at Site PS2644, where the inflow to the DK Strait was constricted like in a funnel. The enhanced current regime is also documented at the end of GI 2, during the B/A, and major parts of the Holocene, by contrast to today, where a thin layer of few cm modern sediment is still preserved and^{14}C dated (Voelker, 1999).

During time segment 4, features of DSO mode 3 were fundamentally different from LGM DSO modes 1 and 2. Apart from just medium high ventilation ages mode 3 shows a broad range of intermediate epibenthic $\delta^{13}C$ values (0.6–1.4 source water ventilation, possibly due to a modest HS-1 input of remineralized organic carbon. DSO mode 3 starts with a significant, almost abrupt 0.8 equivalent to a 3.4°C rise in minimum bottom water temperature, that occurred near the actual end of a last high in bottom water ventilation age (Fig. 4). The diverse range of $\delta^{18}O$ data of epibenthic single species could reflect a broad array of bottom water temperatures for each sediment sample extending over 1.5–2.0 to about 8°C. Since this range appears unlikely, it probably includes an imprint of $\delta^{18}O$ signatures of waters from different seasons and short-term changing source waters.

Per analogy to the records of PS2644, Sessford et al. (2018) report on Mg/Ca-based bottom water temperatures for stadial and interstadial periods over MIS3, analyzed in twin sediment core GS15-198-36CC. Here, minimum values of 1° to -1.5°C mark Greenland Interstadials (GI) 5, 6, 7, and GI 8, when bottom waters

were formed by convection in the Nordic Seas, whereas warm temperatures of 2°–4°/ 5°C marked Greenland Stadials (GS) 4, 5, 7, 8, and the very onset of GI 8. Temperature anomalies reached up to 6°C and provide crucial evidence for short-term substantial changes in the origin and circulation geometry of DSO waters during MIS3, similar to those deduced in our study.

Last but not least, DSO mode 3 goes along with a significant rise in εNd and drop in $^{206}Pb/^{204}Pb$ isotope ratios, in particular during time segment IV (Figs. 4 and 5). The proxies form an important tracer of basaltic sediments from Iceland and/or the Iceland-Scotland Ridge, predominantly passed by mode-3 waters prior to reaching Site PS2644 (˜68°N) at the northern entrance of the Denmark Strait, similar to the modern track of the "North Iceland Jet" (Våge et al., 2011). Less likely, the isotope ratios may trace East Greenland basalts (S of 70°N) (Peate and Stecher, 2003), since the EGC acts as interjacent barrier (Fig. 1).

During time segment III, the flow strength of DSO mode 3 may have been similar to that of the preceding mode 2. During time segment IV, however, it may have decreased significantly or may have even been negligible, when meltwater advection reached a final maximum and hemipelagic bulk sedimentation rates at Site PS2644 displayed an abrupt rise by a factor of 3 to 5 (Fig. 4). The high sedimentation rates were paired with abundant ice-rafted debris (IRD) rich in hematite-stained red quartz grains that depict an ongoing flux of Devonian 'Old Red' sediments picked up by icebergs along the N.E. Greenland margin (N of 72°30'N), hence reflect a continued afflux of the EGC (Voelker, 1999).

In search for a hypothetical ultimate source of DSO mode 3 waters during HS-1, sediment proxies provide several independent lines of evidence for a link to the topmost intermediate and/or subsurface waters in the (then possibly sea-ice covered) Atlantic south and southeast of Iceland: (i) Their dominant minimum epibenthic $\delta^{13}C$ values of 0.6-0.9 output of peak glacial DSO modes 1 and 2. However, they largely resemble the low $\delta^{13}C$ values of 0.2 - 0.9 output south of the Denmark Strait (at ˜2000 m w. d. during late HS-1, in addition to some rare $\delta^{13}C$ outliers of single specimens that record local brine water formation in the Irminger Sea (-0.2 to -1.5 2002; Sarnthein et al., 1994). (ii) The ventilation age range recorded for DSO mode 3 during time segments III and IV (Fig. 4) matches closely that reported for subsurface and intermediate waters south of Iceland (Thornalley et al., 2011). (iii) Though *per se* largely unknown, the minimum temperatures of topmost Atlantic Intermediate Waters (that, as we surmise, crossed the western Iceland-Scotland Ridge with the NIJ at depths of <200 m w. d.) have definitely been much higher than those of polar waters probably entrained at Site PS2644 along with LGM DSO modes 1 and 2 (e.g., coeval abrupt 1-$\delta^{18}O$ values at Site SO82-5 south of Iceland, ˜1400 m w.d.; van Kreveld et al., 2000) and per analogy to today. (iv) As outlined above, the highly radiogenic εNd values of DSO mode 3 could mean an antecedent passage over basaltic sediments as found on the Iceland-Faeroe Ridge and northern slope of Iceland, defined as "North Iceland Jet" by Våge et al. (2011), which today supplies almost half of the total DSO flow rate (Figs. 1 and 6).

Variable DSO modes linked to short-term changes in surface water composition

On centennial timescales, the immense shift from peak glacial DSO modes 1 and 2 to deglacial mode 3 was directly paired with the distinct onset of a $\delta^{18}O$ depletion of (sub-) surface waters at PS2644. It started right at the base of deglacial time segment III, 18.4 cal. ka, subsequent to a long-term constant LGM $\delta^{18}O$ maximum near ˜4.5 ˜22.0 cal. ka (Fig. 4). The start of a gradual decrease in planktic $\delta^{18}O$ by up to 1.5 both warmer and meltwater-diluted surface waters advected through the Denmark Strait, a precursor of the North Iceland branch of the Irminger Current. After 17.2 cal. ka, the shift resulted in an SST rise by 2°–4°C during time segment IV (based on census counts of planktic foraminifera of Voelker, 1999; Pflaumann in Sarnthein et al., 2001; Hagen and Hald, 2002). The rise was paired with a meltwater-induced salinity reduction that necessarily led to continued sea ice cover (You et al., 2023; Sadatzki et al., 2020). Thus, any local CO_2 and ^{14}C exchange between atmosphere and surface waters off East Greenland was continuously suppressed until ˜15.1 cal. ka (Fig. 2a).

Changing surface waters and deep-water formation in the eastern Nordic Seas

In the eastern Nordic Seas, by comparison, planktic $\delta^{18}O$ values of 4.6–4.8 HS-1 meltwater signal over the LGM and most of HS-1, from 18.4–16.3 cal. ka, except for a minor $\delta^{18}O$ low ˜17.6–17.2 cal. ka (by $\Delta\delta^{18}O$

= 0.3 Fig. 2b). Figs. 2b and 3, however, display an almost sudden 2-the planktic $\delta^{18}O$ record, that clearly document – after the first incursion of meltwaters at PS2644 in the west – a second major ice and meltwater outbreak during the last 1000 yr of HS-1a starting at 16.3-16.0 cal. ka (as with the onset of HS-1b, precisely coeval with a second major HS-1 cooling depicted in Greenland ice cores GRIP2 and NGRIP). The meltwater signal started from the Barents shelf, spread south down to Faeroe (Sarnthein et al., 2001). The ice breakout obviously induced a turbulent mixing down to intermediate waters at Site GIK23074 at 1157 m w. d. (Fig. 3), and lasted until ˜14.7 cal. ka. This age estimate on top of HS-1a fits precisely a $\delta^{18}O$ depletion found in Greenland records NGRIP and GISP2 (e.g., Grootes and Stuiver, 1997).

Over time segments I and II, **eastern surface waters** showed fairly **low MRA** of ˜500 to 800 and 1200 yr (Figs. 2b and 3 that closely resemble MRA values recorded for the very early LGM by Simon et al. (2023). However, they differed strongly from the high MRA of 1900-2200 yr obtained from Site PS2644 in the west (Fig. 2a). Starting at 18.4 cal. ka, however, eastern MRA depict a fast rise to 1730 yr and 2000 yr, rapidly reaching a close match with the MRA found at western Site PS2644 over time segment III and early segment IV (Fig. 2b). Accordingly, the differential sense of eastern and western surface water circulation of time segments I and II ended and was briefly replaced by a close match during time segments III and IV, when 'old' surface waters with an Arctic origin similar to those of the EGC had started also to cover the eastern Nordic Seas. Per analogy, we infer that this advection dominated until ˜16 cal. ka.

During time segment I, extremely **low bottom water ventilation**ages at Site GIK 23074 attest lively intermediate-water convection somewhere close to the site in the eastern Nordic Sea at least down to ˜1200 m w.d. (Figs. 3 and 6; in harmony with Meland et al., 2008; Thornalley et al., 2015). In contrast, the regime at Site PS2644 was stratified. Occasionally, extremely young intermediate waters of Site GIK23074 found their way from the east up to the west, at Site PS2644 forming DSO mode 1 during time segment II (Fig. 4), where local deep-water convection continued in the eastern Nordic Seas, though somewhat attenuated (Fig. 3).

After 18.4 cal. ka, with the start of time segment III, the circulation geometry of the eastern Nordic Seas was strongly modified (Fig. 6; modified after Thornalley et al., 2015). The**inflow of NAC** stopp**ed** . It was r eplaced by surface waters with high and very high MRA at Site GIK23074 / MD95-2311 (1157 m), that closely equate the MRA at Site PS2644 reflecting the EGC. Hence, the waters were probably Arctic-sourced. Their arrival was precisely coeval with the start of meltwater incursion through the Denmark Strait (Figs. 3, 4). Local intermediate and deep-water convection (*sensu* Siedler et al., 2001) then was replaced by stable stratification and dominantly seasonal, probably fairly modest volumes of brine-enhanced shelf waters leading to modest deep-water formation (Bauch and Bauch 2001; Waelbroeck et al., 2011; Thornalley et al., 2015). This shift is reflected by a local abrupt rise in bottom water ventilation ages from <1000 yr up to 2100-2200 yr, ages that slightly exceed the paired, likewise strongly raised MRA of surface waters reaching 1900-2100 yr (Fig. 3). In turn, the great iceberg and meltwater outbreak from the Barents Sea after 16.3 cal. ka obviously resulted in local stirring and an immediate overturning and renewed local ventilation of intermediate waters in the eastern Nordic Seas (Fig. 3).

Different from a model of Sessford et al. (2019), the brine water-induced intermediate waters of the eastern Nordic Seas during time segments III and IV apparently did never spread up to the westernmost Nordic Seas to replace DSO waters at Site PS2644. Our benthic ventilation ages and other proxy data suggest that the circulation geometry of the west was different from today being dominated by the North Iceland Jet (*sensu* Våge et al., 2011) that entrained DSO mode-3 waters from the east along the northern slope of Iceland and ultimately, from upper North Atlantic Intermediate Waters to the south and southeast of Iceland.

Differential DSO modes and Nordic Sea stratification – Implications for short-term glacial-to-deglacial climate change in the northern hemisphere

After ˜18.4 cal. ka (note: before 1950 AD) (Figs. 2a, 4), intermediate waters ultimately derived from upper intermediate and/or subsurface waters in the North Atlantic started to dominate DSO mode 3 at Site PS2644 north of Iceland below a layer of highly aged, less saline, and southward flowing Arctic surface waters. This

switch in bottom water circulation in the Icelandic Sea was precisely coeval (i) with a very first incursion of meltwaters through the Denmark Strait and (ii) with a pertinent switch in the geometry of surface and intermediate-water circulation in the Norwegian Sea, that is, coeval within the error range of the ^{14}C plateau tuning technique (Figs. 4 and 5) (Sarnthein et al., 2020).

The overall switch from an anti-estuarine to a weakened anti-estuarine flow regime was almost instantaneous, taking from 18.7-18.39 cal. ka. It presented a tipping point in circulation geometry of the complete Nordic Seas, and in turn, of AMOC (e.g., major abrupt rise of MRA near to the Azores Islands; Balmer and Sarnthein, 2018). Accordingly, the switch triggered a prompt breakdown of the poleward advection of warm Atlantic surface waters, that previously had driven the "Nordic Heat Pump" up to northern Norway and Svalbard over peak glacial time segments I and II per analogy to today, though with somewhat lower SST (based on % Nps and Artificial Neural Network = ANN records of Weinelt et al., 2003). We are confronted with a tipping point in North Atlantic circulation geometry and climate, that marked already the onset of the HS-1b cold spell at a very early tie point in deglacial time. Below, the age and potential time span covered by the oceanographic shift itself are compared with the climate history constrained by temperature records on Greenland in ice cores, independently dated with an incremental time scale based on annual-layer counts.

Based on the NGRIP δ^{18}O record (GICC05; Wolf et al., 2010), the temperatures in North Greenland reflect an overall trend of gradual deglacial warming from 22 to ˜17 cal. ka (Figs. 4 and 5). The trend, however, was interrupted by a significant first deglacial breakdown in the advection of warm atmospheric moisture, an event here named 'HS-1b' that started between 18,500 and 18,380 cal. yr ago (before 2k). The event was less distinct in ice core GISP2, here depicted between 18,630 and 18,430 cal. yr b2k (Grootes and Stuiver, 1997). This age range matches within the range of a century the great switch in seawater stratification of Nordic Sea circulation independently measured at two different marine sediment records at the base of time segment III, when dated by means of ^{14}C plateau tuning. *Per se* , the age match may form a proof for the robustness of ^{14}C plateau-based age estimates. Also, the event is reflected directly by a short atmospheric^{14}C plateau named '4a' lasting from ˜18.6 to ˜18.4 cal. kyr before 1950 AD (Figs. 2a and b; Sarnthein et al., 2023). Based on GICC05 ages, the fundamental switch in seawater stratification and the resulting drop of the Nordic heat pump may have taken no longer than 80–100 yr.

Unfortunately, it is widely impossible to compare this narrow age range with any of the numerous IRD and SST records published for the onset of HS-1 from the North Atlantic "Heinrich-1 IRD Belt". Except for some sporadic and wide-spaced single age tie points (Hodell et al., 2017, and refs. therein), local MRA levels and even more so, the precise timing of their short-term variations are largely unknown due to a lack of sediment records with absolute datings such as high-resolution^{14}C plateau tuning. By comparison to pertinent changes recovered in the Nordic Seas over HS-1 (Figs. 2a and b) local MRAs may actually have shown short-term variations between 200 and 2000 yr. Also, the age range of meltwater advection and ice-rafted debris input was subject to major regional variations, while winds and currents were driving icebergs over vast sea regions. Off southwestern Portugal, for example, sediment record SHAK06-5K the ages of which were calibrated by^{14}C plateau tuning (Ausin et al., 2021) show a δ^{18}O-based local meltwater incursion and an IRD input not starting prior to 17.8/17.9 cal. ka, that is 500-600 yr after the start of HS-1b, as defined in our Nordic Seas cores. – During the Alpine Late Glacial, the HS-1 cold spell is reflected by the well-dated "Gschnitz Stadial" that showed temperatures and aridity closely similar to those estimated for the LGM (Ivy-Ochs et al., 2023).

CONCLUSIONS

* On the basis of the ^{14}C PT technique we define a suite of four peak glacial to early-deglacial time segments from 22-15 cal. ka, that show differential MRAs and bottom water ventilation ages at two core sites in the western and eastern Nordic Seas.

* On the basis of sediment-based quantitative proxy-data we distinguish three glacial-to-deglacial modes of Denmark Strait Overflow (DSO), each of them revealing differences in source region, formation mode,

and/or in flow intensity.

* The proxy records suggest that waters of DSO modes 1 and 2 were largely fed by a mix of Arctic intermediate waters and deep-water convection in the eastern Nordic Seas, either reflecting a weaker (mode 2) or stronger and even erosive (mode 1) anti-estuarine flow geometry at the northern entrance to the Denmark Strait, similar to today.

* Starting at 18.4 cal. ka, the proxy records of time-segments III and IV show a meltwater-diluted Irminger Current that entered the Denmark Strait from southwest. It induced an immediate switch to DSO mode 3, then dominated - as we hypothesize - by subsurface and upper intermediate waters advected from the northern North Atlantic southeast of Iceland, hence suggesting a strongly weakened anti-estuarine flow geometry.

* Near 18.4 cal. ka, the climate tipping point between DSO modes 2 to 3 is marking the onset of Heinrich stadial 1b. This switch in ocean flow geometry caused a temporary end of the Nordic Heat Pump. The switches took hardly more than a century, a time span independently confirmed by incremental age estimates obtained from the Greenland temperature records of GISP2 and NGRIP.

* The fundamental switch in Nordic Seas flow geometry ˜18.6–18.4 cal. ka is also reflected by a special atmospheric ^{14}C plateau, by ^{14}C plateau 4a.

* After 16.3 cal. ka, a subsequent meltwater outbreak from the Barents shelf (Weinelt et al., 1991) caused a major prolongation of the HS-1 flow geometry in the Nordic Seas and further cooling of HS-1, then named Heinrich stadial 1a until Dansgaard-Oeschger Event 1, independently documented in Greenland ice core records (˜16.1 – 14.7 cal. kyr b2k).

IMPLICATIONS

The onset of cold spell HS-1b forms a scenario enticing to speculate about potential trends found today and in the near future (e.g., in view of models of Ditlevsen and Ditlevsen, 2023; Jansen et al., 2020; Caesar et al., 2018) on the basis of following boundary conditions: (i) Within few decades the onset of the cold spell near 18.4 cal. ka was found coeval at two records from Greenland ice cores and two marine sediment records that showed a fundamental switch from anti-estuarine to modified sources of anti-estuarine flow geometry in the western and a switch to weak anti-estuarine in the eastern Nordic Seas and accordingly, also in AMOC. (ii) The tipping point of seawater stratification was met as soon as first meltwaters had arrived through the Denmark Strait. (iii) The switch to estuarine and/or weak anti-estuarine flow geometry in the Nordic Seas and consequentially, the breakdown of Nordic Heat Pump took probably less than 100 yr.

In turn, however, we don't have any evidence for the actual source of these meltwaters somewhere in the Irminger and Labrador Seas. Even less, we can quantify the past meltwater fluxes needed to trigger the almost abrupt onset of HS-1b by comparison to meltwater fluxes from Western Greenland and Baffin Island, that today are admixed to the North Atlantic Drift and finally may serve as potential origin of a future tipping point in AMOC geometry. Thus, the analog of the start of HS-1 is left with open questions.

Data availability

All primary radiocarbon data and cal. ages assigned are stored at PANGAEA.de® under "still to be processed".

,,,

ACKNOWLEDGMENTS

We thank Pieter M. Grootes, Kiel, and Antje Voelker, Lisboa, for substantial critical comments on our manuscript and for references to recent publications. In particular we thank A. Biastoch, Kiel, for his advice in potential questions of physical oceanography. We gratefully acknowledge the help of Ralf Tiedemann, AWI Bremerhaven, with the acquisition of special additional sediment samples from Core PS2644, John Southon, Irvine CA, and Gesine Mollenhauer, AWI Bremerhaven, for analyzing ^{14}C ages of benthic foraminifera

samples of Core GIK23074, and Michael Bollen for help with the analysis of Nd and Pb isotope data at the University of Lausanne. Sebastian Beil, Kiel, and Hugo Ortner, Innsbruck, kindly helped us with software problems. P.B. acknowledges funding from the European Union's Horizon 2020 research and innovation program (grant agreements No 101065424, project OxyQuant).

FIGURE CAPTIONS

Figure 1. Location of twin sites PS2644 and GS15-198-36GC in the Icelandic Sea (67°52'N, 21°46'W, 777 m w.d.) and twin sites GIK23074 and MD95-2311 in the Norwegian Sea (66°40'N, 4°54'E, 1157 m w.d.). Yellow arrows mark warm surface water currents entering the Nordic Seas (NAC: North Atlantic Current, NIIC: North Iceland Irminger Current), green arrow shows the EGC. Arrows on top of broken lines depict intermediate-water currents such as the Denmark Strait Overflow (DSO), the North Iceland Jet (NIJ), and the Iceland Scotland Overflow Water (ISO). Bathymetry based on Ocean Data View (Schlitzer, 2002), highlighted by faint 250-m isoline.

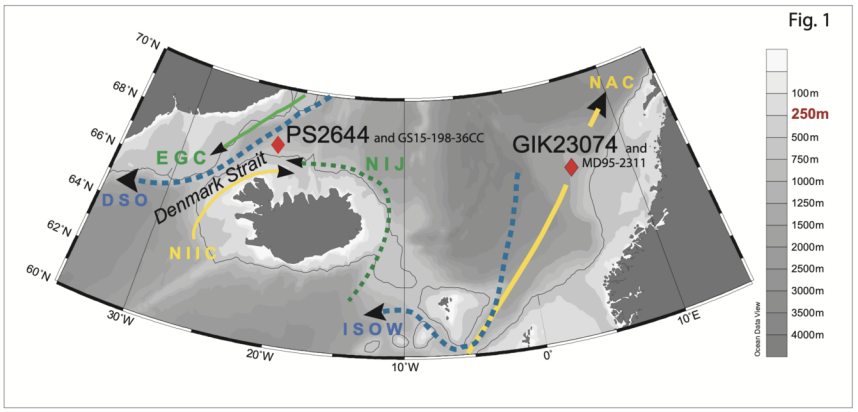

Figures 2a and b. Planktic 14C records of sediment cores PS2644 and GIK232074 plotted vs. core depth; for core locations see Fig. 1. Planktic 14C plateaus (horizontal boxes) are compared to atmospheric (atm) 14C plateau suite of Lake Suigetsu (Bronk Ramsey et al., 2020), where calendar ages of plateau boundaries (and average atmospheric 14C ages) are given below in cal. ka BP (before 1950 AD). Atmospheric plateau 4a directly reflects the switch in Nordic Seas flow geometry ˜18.6–18.4 cal. ka (before 1950 AD). Local planktic reservoir ages (in blue) result from the difference between the average raw 14C age of planktic 14C plateaus measured in the core and the 14C age of equivalent atmospheric ^{14}C plateaus numbered 1 – 6 (numbers in brackets). Top panel shows units of the 1st derivative (14C yr per m core depth) and 1-σ uncertainty range, with high values indicating 14C jumps and 14C plateaus (numbered in red) constrained at 'half-height' by asterisks (as defined in Sarnthein et al. 2015). Green dots display paired benthic ^{14}C ages. B/A = Bølling-Allerød; HS-1a+b = Heinrich Stadial 1 a and b; LGM = Last Glacial Maximum. Sedimentation rates are based on cal. ages of 14C plateau boundaries. Red dotted line in Fig. 2b shows local planktic δ^{18}O record of *N. pachyderma* sin. (Voelker, 1999)

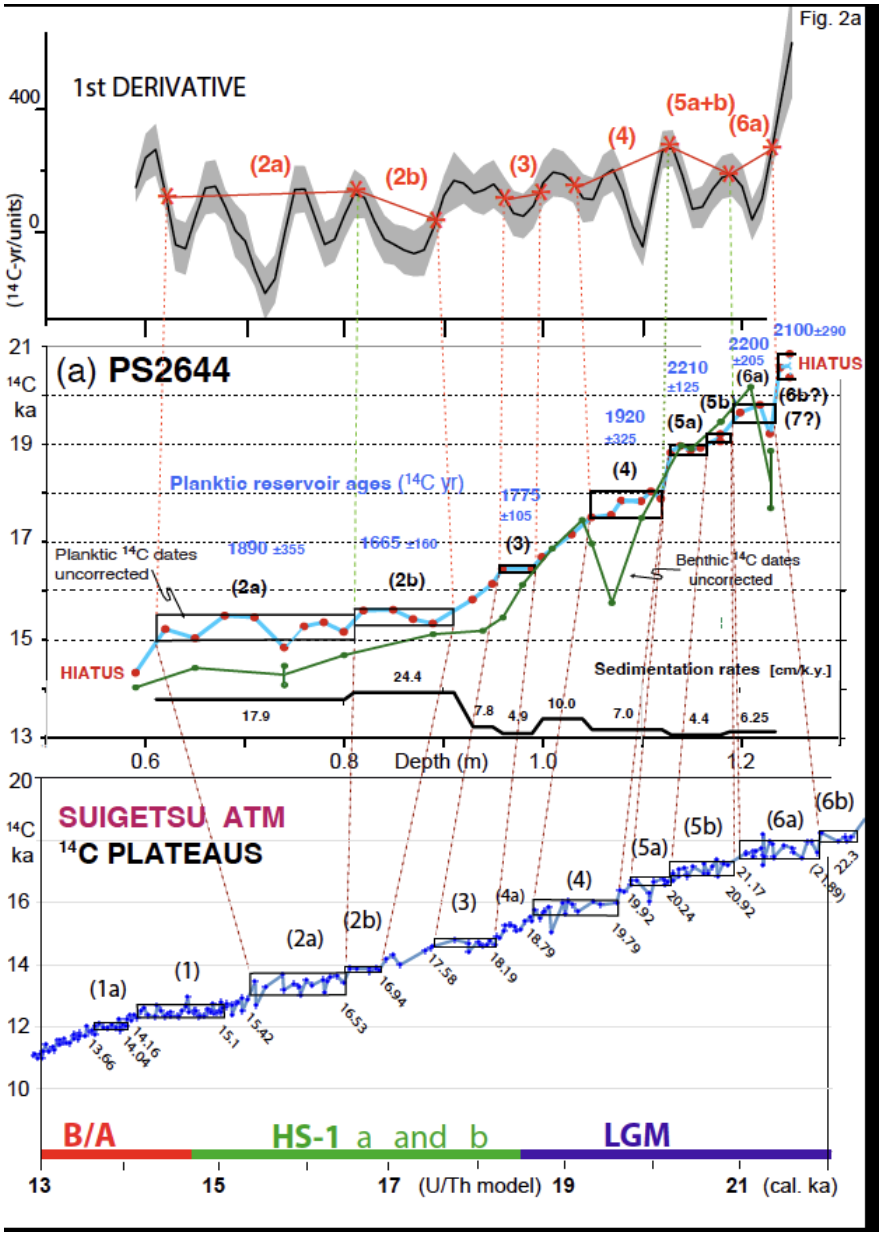

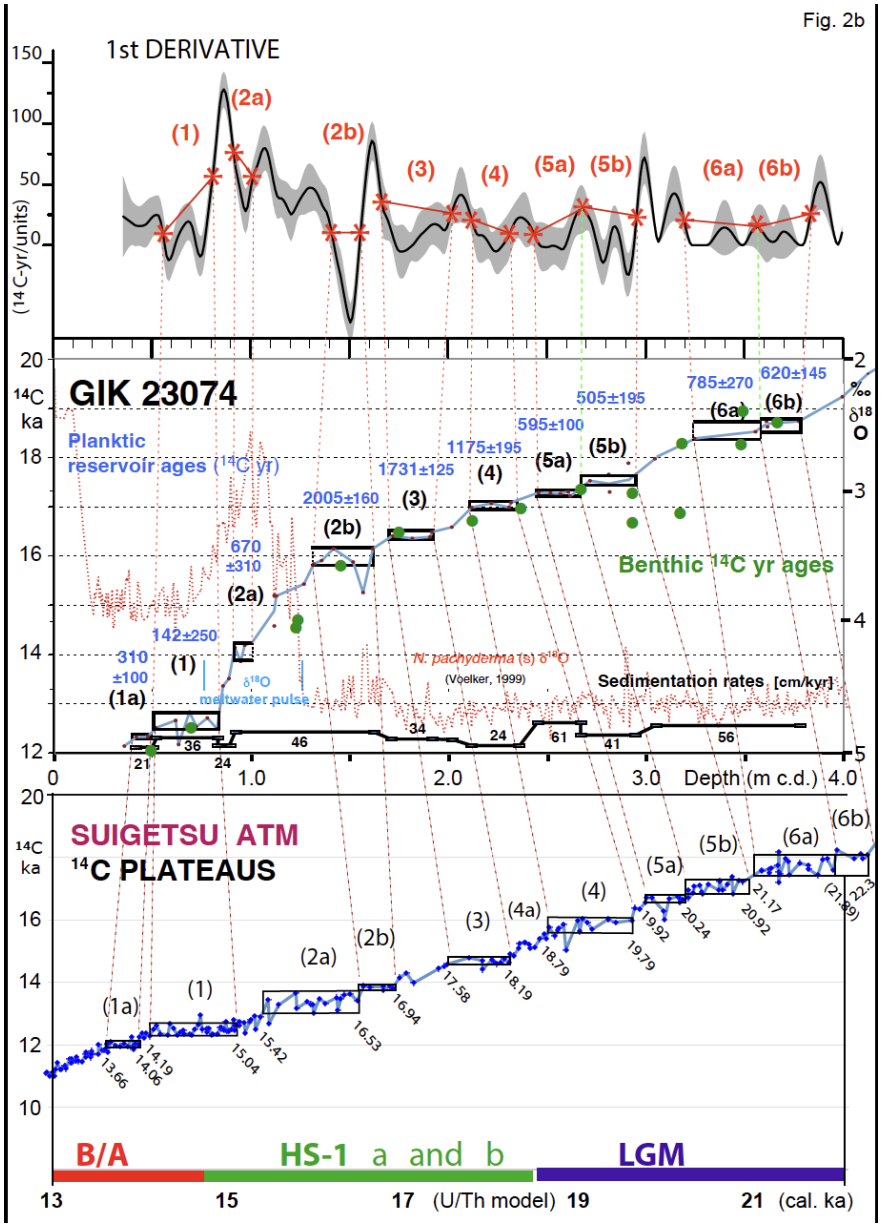

Figure 3. Top panel: NGRIP δ^{18}O record vs. cal. ka b2k (GICC05, Wolff et al., 2010) as reference to centennial-scale climate changes in the northern hemisphere. Second panel: Prominent late-HS-1 minimum in planktic δ^{18}O record of Core GIK23074 records meltwater breakout from Barents Shelf ice, also reflected by a distinct cooling of HS-1a (topmost panel). Third panel: Planktic reservoir ages ("MRAs"; blue) and benthic ventilation age records (red) of sediment core GIK23074 document peak glacial-to-deglacial changes in surface and bottom water oceanography in the Norwegian Sea 23 – 13 cal. ka (before 1950 AD). Benthic ^{14}C ages are based on specimens of *Cribrononion teretis* only. Blue and red asterisks mark two cal. age estimates of planktic and benthic foraminifera based on paired U/Th ages of a solitary coral (Dreger, 1999, plus unpubl. written comm. 2000). Lowermost panel: Planktic reservoir ages ("MRAs"; blue) and benthic ventilation age records (red) of sediment core PD2644 document peak glacial-to-deglacial changes in surface and bottom water oceanography in the Icelandic Sea 22 – 15 cal. ka (before 1950 AD). Benthic ^{14}C ages are based on specimens of epibenthic *Cibicidoides lobatulus* . —- Roman numbers show time segments I to IV.

Note, age scales of GIK 23074 and PS2644 records have not been aligned to the age scale of NGRIP but are independently based on atmospheric ^{14}C plateau tuning.

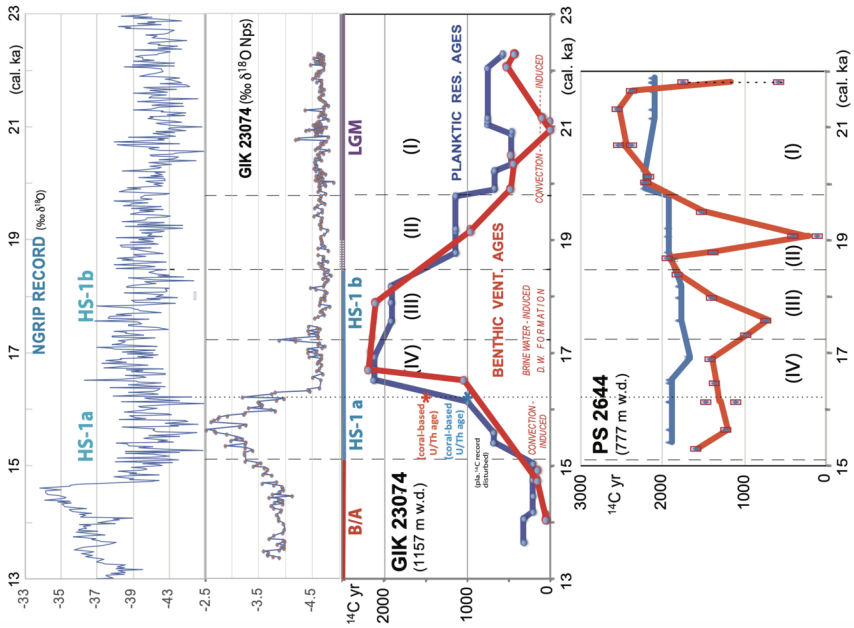

Figure 4. Comparison of various proxy records from sediment core PS2644 that document peak glacial-to-deglacial changes in surface and bottom water oceanography at the northern entrance of the Denmark Strait 22 – 15 cal. ka (before 1950 AD). Age control based on ^{14}C plateau tuning technique. Top panel shows NGRIP δ^{18}O record of Greenland vs. cal. ka b2k (GICC05; Wolff et al., 2010) as reference to coeval changes in northern hemisphere climate plotted vs. planktic δ^{18}O record of SST rise and meltwater dilution of NIIC waters (Voelker, 1999). Roman numbers indicate time segments I to IV. Panel 2 shows planktic reservoir ages (i.e., MRA; red broken line), prominent changes in benthic ventilation age (blue line; Sarnthein et al., 2020), and two separate populations of epibenthic δ^{13}C values obtained from single foraminifera tests (Voelker, 1999). Panel 3 depicts epibenthic δ^{18}O values of single foraminifera tests (Voelker, 1999), where a 0.8 shift in maximum δ^{18}O reflects an abrupt 3.4°C rise in minimum bottom water temperature near 18.4 cal. ka. Panel 4 shows gradual rise in the radiogenic ε_{Nd} portion of Nd isotopes of authigenic and detrital sediment fractions as compared to modern and mid-Holocene (”Oetzi time” ˜5.7 cal. ka) values (Kutschera, 2002). Panel 5 shows variations in authigenic and detrital Pb206/Pb204 ratios. Panel 6 gives changes in bulk sedimentation rate (cm/kyr) as derived from cal. ages obtained by means of the^{14}C plateau tuning technique (Sarnthein et al., 2020).

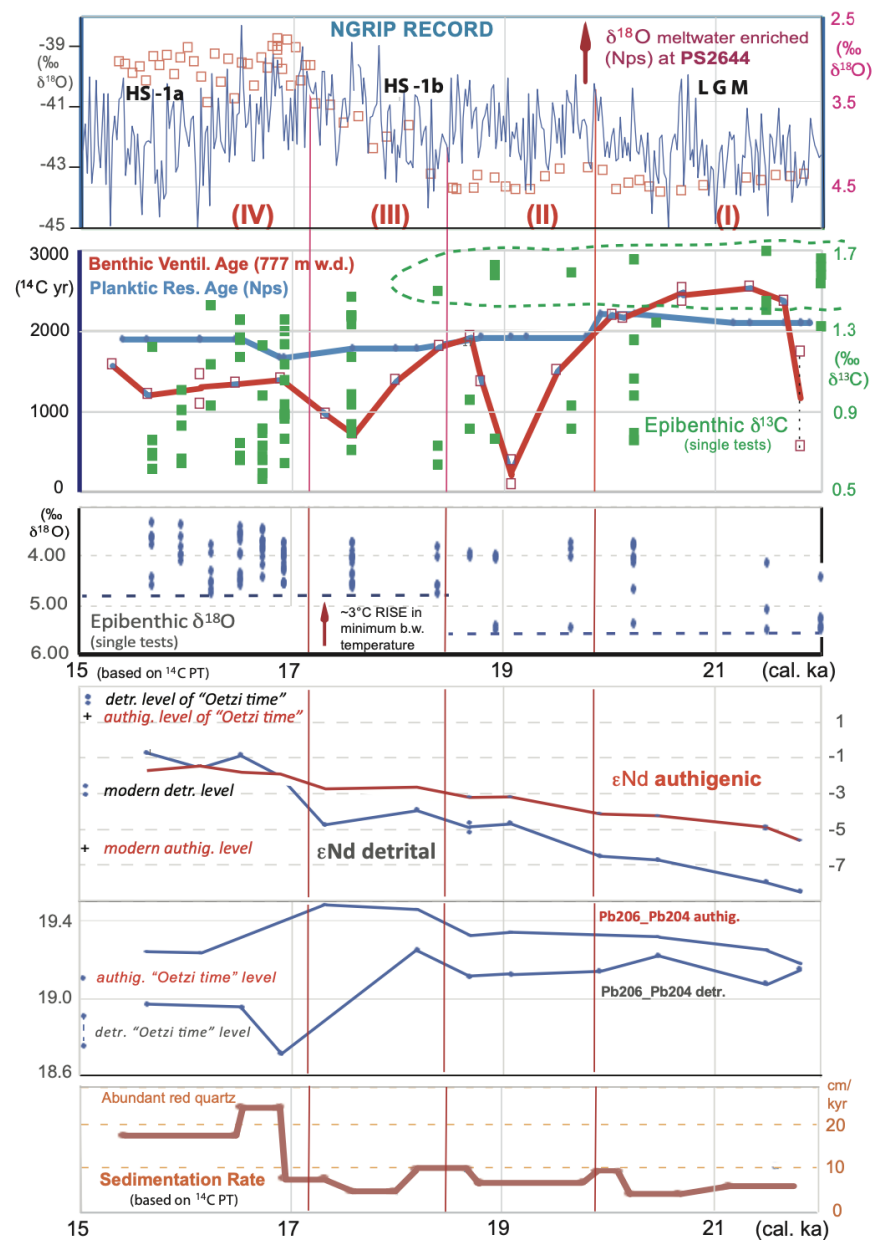

Figure 5. Authigenic and detrital $^{206}Pb/^{20}4Pb$ ratios vs. eNd at Site PS2644 and potential sediment sources. PS2644 data are symbols indicate different time segments as described in the text. The Holocene sample was derived from a combination of eNd data at the core top and Pb isotope data from an ash layer at 18 cm depth, since the core top appeared to be contaminated by strongly unradiogenic anthropogenic lead. Potential end members are indicated as shaded areas (Crocker et al., 2016; Crocket et al., 2012; Eisenhauer et al., 1999; Fagel et al., 2002; Farmer et al., 2003; Haley et al., 2008; Kempton et al., 2000; Peate and Stecher, 2003; Struve et al., 2019). Data from ODP Site 980 in the Northeast Atlantic are from authigenic sediment fractions only. Greenland isotopic ratios span large ranges outside the limits of the figure.

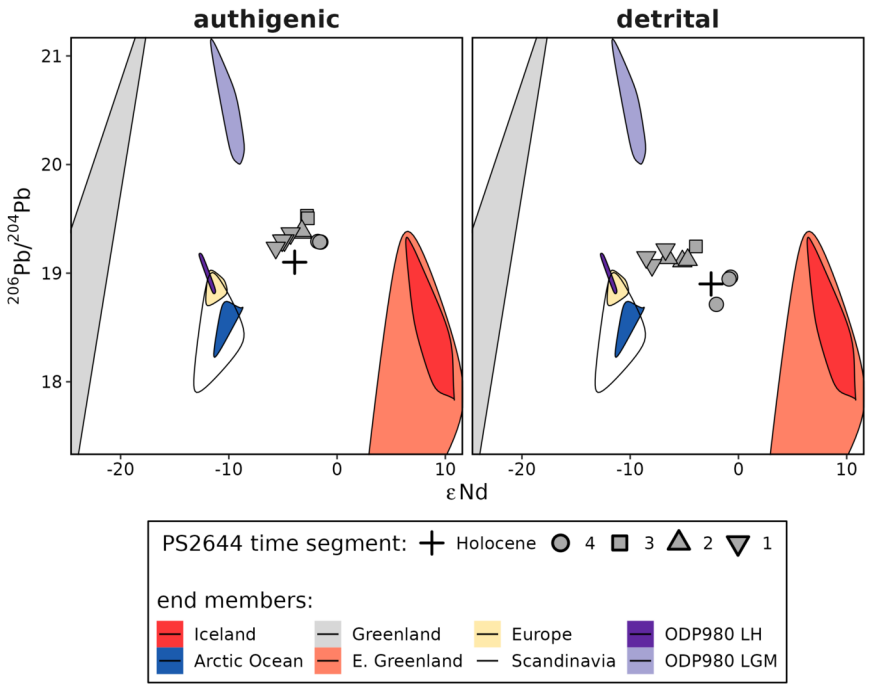

Figure 6. Scheme showing vertical transects of hypothetical circulation geometry across the western and eastern Nordic Seas between North Atlantic, Greenland-Island (GI) / Island-Scotland (I-S) Ridge, and Fram Strait (schemes modified from Thornalley et al., 2015), showing deep- and intermediate-water convection separately for the eastern (lower panel) and western (upper panel) Nordic Seas. Grey arrow colors indicate brine water-induced intermediate waters and weak anti-estuarine overflow. Transect (A) for LGM, transect (B) for HS-1 times starting at 18.4 cal. ka. Red asterisks: Core sites PS2644 and 23074. Red numbers give prime evidence, the range of local planktic reservoir ages (MRA) and benthic ventilation ages. Pertinent MRA and bottom water ventilation ages for core sites RAPID-10-1P and RAPID-17-5P south of the Iceland-Scotland Ridge are from Thornalley et al. (2011). SSDW = Southern Source Deep Water, GA SSW = Glacial Atlantic Southern Source Waters, NIJ = North Iceland Jet, DSO = Denmark Strait Overflow, ISO = Iceland Strait Overflow, EGC = East Greenland Current. Estimates of full and partial sea ice cover for LGM and Heinrich transects are based on Sadatzki et al. (2019), and Sessford et al. (2019).

Note, in our view, MRAs and benthic ventilation ages listed by Thornalley et al. (2011 and 2015) and in part incorporated in Fig. 6B may not reflect true past values (1) because of a lack of precise atm. age calibration (leading to little evidenced MRAs), (2) since a majority of age samples were based on *Pyrgo* , etc. species which are strongly subject to the bias of "old" pore waters in the ambient sediment (Magana et al., 2010).

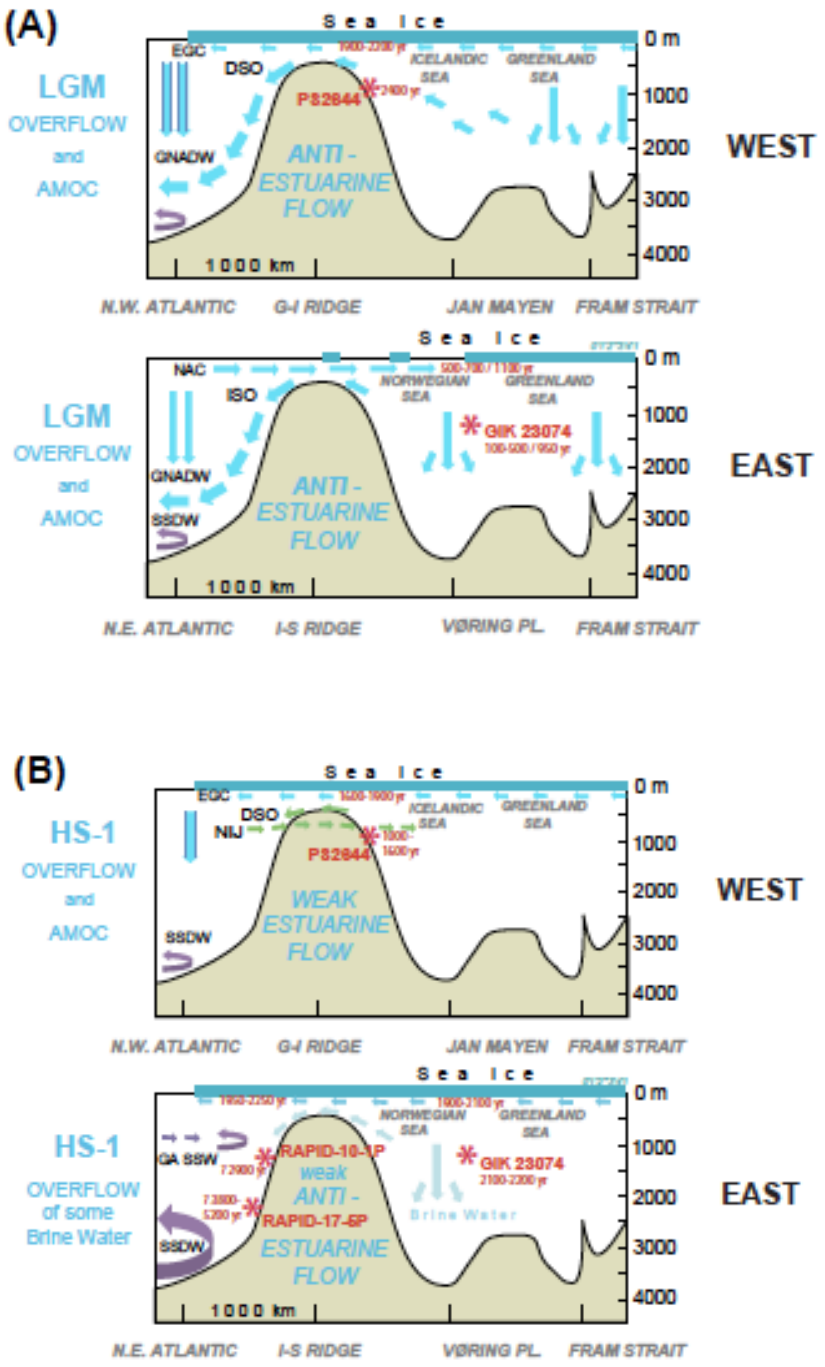

Figure S1. Stratigraphic alignment of structures in planktic $\delta^{18}O$ record and various further proxy records of PS2644, correlated for detailed age derivation to $\delta^{18}O$ record of GISP2 dated on the basis of annual-layer counts (copy of Voelker, 1999).

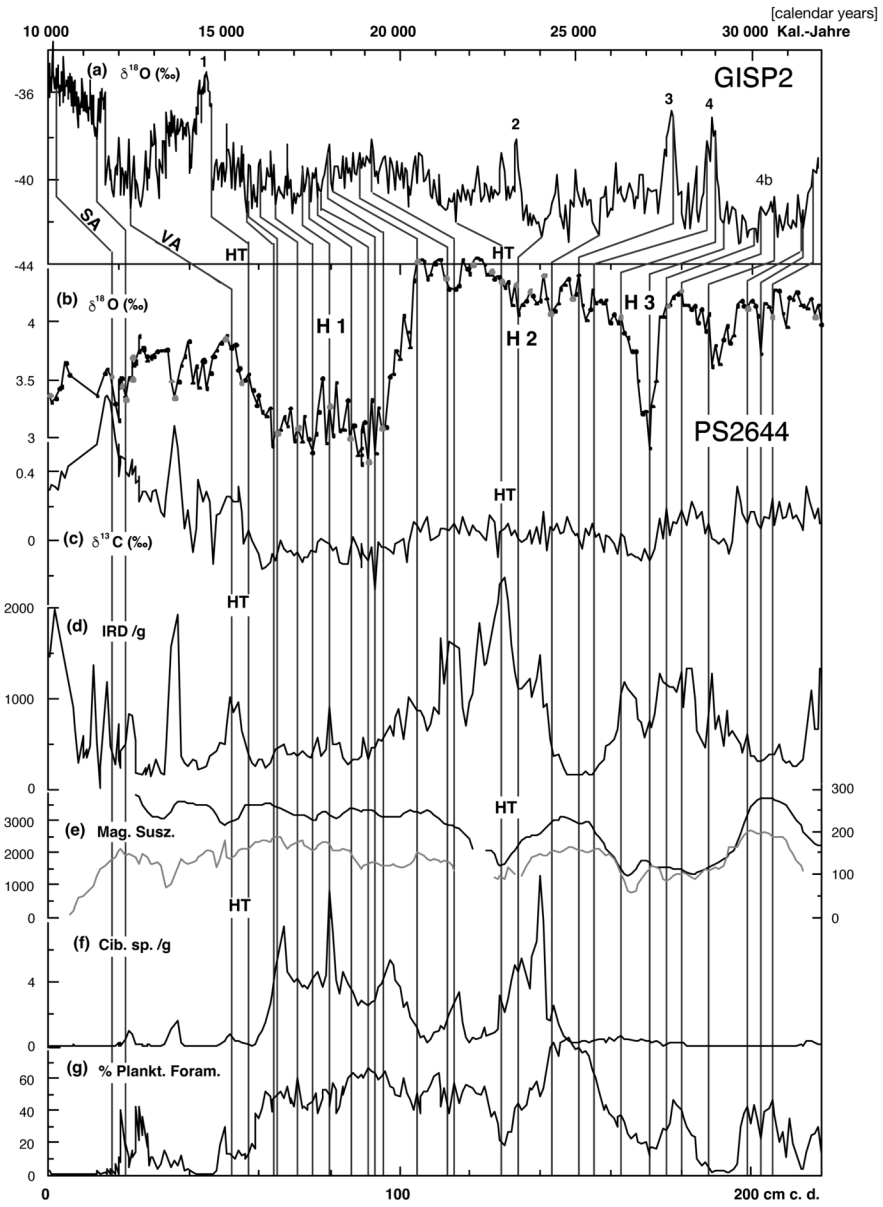

TABLES

Table 1: Listing of planktic and benthic ^{14}C ages, age tie points derived from ^{14}C plateau tuning, MRA, and benthic ventilation ages deduced for sediment cores Core PS2644 (Table 1a) and Core GIK23074 (Table 1b).

PS 2644-5 67°52'N, 21°46'W, 777 m w.d.)

						estimated						r a w
Labcode	**Midpoint Core Depth (cm)**	**Raw Plankt. 14C age *(N.pachyderma s)* (yr BP) (revised 2011)**	**Error (1s) (±yr)**	**SUIGETSU Plateau No. top / base**	**Cal. ages tuned to Suig.U-Th (kyr BP) IntCal20 BOLD: Plateau bound. ages**	**Sedim. Rate cm/ky _yr/cm IntCal20**	**MRA_Plankt. Res. Age vs. Suigetsu (14C yr)**	**Labcode**	**Raw Benthic 14C age *Cibi.wuell.* (yr. BP)**	**Error (1s) (±yr)**	**Benthic-Planktic Age Difference (14C yr)**	**Be. Vent. Age vs. Suigetsu (14C yr)**
	HIATUS											
KIA 802	59	14366	75		15305		1890	KIA 741	14049	82	-315	1575
	61	——		2a top	**15415**	**17.94**	1890					
KIA 29415	62	15260	75	2a	15471	_55.7	1890					
KIA 77	65	15081	162	2a	15638		1890	KIA 1649	14450	80	-630	1210
KIA 29416	68	15540	90	2a	15805		1890					
KIA 29417	71	15510	80	2a	15972		1890					
KIA 736	74	14887	116	2a	16140		1890	KIA 742	14131	82	-750	1090
KIA 743	74	——		2a	16140		1890	KIA 743	14494	89	-390	1450
KIA 29418	76	15320	75	2a	16251		1890					
KIA 29419	78	15405	75	2a	16363		1890					
KIA 78	80	15212	195	2a	16474		1890	KIA 1650	14720	90	-490	1350
	81	——		2a / 2b	**16530**	**24.39**	1890					
KIA 29347	82	15640	70	2b	16571	_41	1665					
KIA 79	85	15659	160	2b	16694		1665					
KIA 29420	87	15470	75	2b	16776		1665					
KIA 737	89	15375	121	2b	16899		1665	KIA 744	15150	90	-230	1400
	91	——		2b base	**16940**	**7.81**	1665					
KIA 29404	93	15870	70		17196	_128						
KIA 43118	94	——			17324			KIA 43118	15170	95	-700	960
KIA 41438	95	16140	100		17452							
KIA 29256	96	16500	85	3 top	**17580**	**4.92**	1775	KIA 43119	15440	90	-1060	715
KIA 45817	98	——		3	17986	_203	1775	KIA 45817	16110	85	-390	1380
KIA 803	99	16507	90	3 base	**18190**	**10**	1775					
KIA 41997	100	16690	100		18290	_100	1775					
KIA 45818	101	——			18390		1775	KIA 45818	16850	100	90	1800
KIA 29346	103	17210	80		18590							
KIA 43662	104	——			18690		1920	KIA 43662	17435	110	0	1920
KIA 41284	105	17500	100	4 top	18790	7	1920	KIA 44984	16950	100	-550	1370
KIA 804	107	17618	113	4	19076	_143	1920	KIA 1641	15790	120	-1810	90
KIA 1641	107	——		4	19076		1920				-1530	390
KIA 41998	108	17840	110	4	19219		1920					
KIA 41285	108	18850	110	4	19219		1920					
KIA 29421	110	17900	100	4	19505		1920	KIA 43663	17480	110	-420	1500
KIA 41286	111	18030	100	4	19648		1920					
KIA 41287	112	17880	120	4 base	19790		1920					
KIA 41999	113	18820	125	5a top	19920	9.4	2210					
KIA 41288	114	18810	110	5a	20026	_106	2210	KIA 43120	17480	110	-20	2190
KIA 42000	114	18980	130	5a	20026		2210					
KIA 805	115	18952	129	5a	20132		2210	KIA 43121	18900	120	-50	2160
KIA 29254	116	19000	110	5a base	20240	4.4	2210					
KIA 29405	118	19130	90	5b ?	20694	_227	2200	KIA 43664	19450	130	320	2520
KIA 29572	118	19280	135	5b ?	20694		2200				170	2370
	119	——		6a top	21170	6.25	2100					
KIA 80	120	19727	245	6a	21330	_160	2100				430	2530
KIA 43665	121	——		6a	21490		2100	KIA 43665	20160	140		
KIA 29345	122	19890	100	6a	21650		2100				270	2370
KIA 806	123	19288	126	6a	21810		2100	KIA 745	17740	160	-360	1740
KIA 806	123	19210		6a	21810		2100	KIA 44986	18850	265	-1530	570
	123.5	——		6a base	21890		2100					
KIA 42001	124	20605	145	6b ?	21970							
KIA 29344	125	20460	110	6b ?								
KIA 29571	125	20940	165	6b ?								
	HIATUS	——			~22000							
KIA 1647	127	21099	152									

AMS ^{14}C ages of planktic and benthic samples were measured at the Leibniz Laboratory, University of Kiel (KIA numbers)

DATA SOUCE: Voelker, 1999, suppl. by 14C ages of
Sarnthein et al., 2015, plus conversion to cal. age estimates of IntCal20 after Bronk Ramsey et al., 2020).

GIK 23074 66°40'N, 4°54'E, 1157 m w.d.

Labcode	Midpoint Depth (cm)	Raw Plankt. 14C Date *(N. pachyderma s)* (kyr BP)	Error (1s) (±yr)	SUIGETSU Plateau No.	MRA_Plankt. Res. Age vs. Suigetsu (14C yr)	U-Th model ages (ka) tuned to (IntCal20)	Sed. rate cm / ky _yr/cm (corr. 2023)	Labcode	Midpoint Depth (cm)	Raw Benth. 14C Date *(C. teretis)*	Error (1s) (±yr)	Benthic-Planktic Age Difference (14C yr)	raw Be. Vent Age (yr)
KIA 705	35.5	12130	70		320	*13368*							
KIA 40194	41.5	12310	80	1a	320	*13656*	18.83						
KIA 1438	47.5	12320	70	1a	320	*13921*	_53						
	49.5	——		1a / 1 top	320	*14065*		UCI 196253	50.75	12070	180	-370	50
KIA 40195	51.5	12500	80	1	210	***14187***	36.13		51.5				
KIA 40196	61.5	12650	90	1	210	*14464*	_27.7						
KIA 41666	63.0	**12160**	100	1	210	*14506*							
KIA 1439	68.5	12820	70	1	210	*14658*							
KIA 41667	72.0	**12530**	95	1	210	*14755*		AWI 1262.1.1	71.5	12,560	45	−55	155
KIA 41668	77.5	**12700**	90	1	210	*14907*							
KIA 41669	82.5	**12480**	100	1 base	210	***15045***	26.1						
KIA 40898	85.5	13350	90			*14160*	_38.3						
KIA 40899	88.5	13500	90			*14275*							
KIA 40197	91.5	14130	90	2a top	685	***15420***	46.35						
KIA 1440	94.5	13850	70	2a	685	*15485*	_21.6						
KIA 40900	96.5	14180	100	2a	685	*15527*							
KIA 41670	99.5	**14220**	90	2a	685	*15593*							
KIA 40198	111.5	15190	100	disturbed									
KIA 41672	111.5	**14570**	120										
KIA 899	112.5	15180	100			*assumed*							
KIA 40902	126.5	15420	120	disturbed		*16530*		UCI 196123	126.4	14,700	60	−1100	1,035
KIA 40199	131.5	15830	100	2b	2135	*16638*							
KIA 1441	135.5	15900	80	2b	2135	*16724*							
KIA 40200	141.5	16140	110	2b	2135	*16854*							
KIA 40201	151.5	15870	110	2b	2135	*16722*		AWI 1263.1.1	150	15,900	30	45	2,180
KIA 1442	156.5	15250	100	2b	2135	*16830*							
KIA 40202	161.5	16140	120	2b base	2135	*16940*							
	170.5	——		3 top	1925	***17580***	33.47						
KIA 40203	171.5	16400	110	3	1925	*17610*	_29.8						
KIA 40204	181.5	16350	110	3	1925	*17908*		AWI 1264.1.1	179.5	16,575	30	170	2,095
KIA 900	190.5	16380	110	3	1925								
KIA 40205	191.5	16480	120	3 base	1925	*18205*							
KIA 40206	201.5	16580	110										
	211.0	——		4 top	1150	***18790***	27.7						
KIA 40207	211.5	16980	120	4	1150	*18826*	_36						
KIA 40208	221.5	17060	120	4	1150	*19170*		AWI 1265.1.1	218.5	16,835	30	−190	960
KIA 901	230.5	16980		4	1150	*19494*							
KIA 40209	231.5	17080	120	4	1150	*18530*							
	235.5	——		4 base	1150	*19790*			235.5				
	244.5	——		5a top	675	***19920***	68.8	UCI 196124	243.75	17080	70	-200	475
KIA 902	245.5	17280	110	5a	675	*19934*	_14.5						
KIA 40258	251.5	17270	80	5a	675	*20021*							
KIA 903	256.5	17260	120	5a	675	*20094*							
KIA 40259	260.5	17300	90	5a	675	*20152*							
KIA 40260	261.5	17210	85	5a	675	*20167*							
	266.5	——		5a/b	675	***20240***	41.67		266.5				
KIA 40261	271.5	17520	80	5b	470	*20360*	_24	UCI 196125	274.75	17490	150	-30	440
KIA 41673	281.0	**17650**	105	5b	470	*20588*							
KIA 41676	281.5	**17295**	125	5b	470	*20600*							
KIA 41674	291.0	**17880**	105	5b	470	*20828*							
KIA 41677	291.5	**17220**	115	**5b**	470	*20840*							
	294.0	——		5b base	470	***20900***	179.4		294.0				
KIA 904	304.5	17970	115			*20958*	_5.6	UCI 191624	301.5	17100	330	−870	−110

KIA 1443	324.5	18380	110	6a top	760	*21070*	36	UCI 191625	326.5	17720	730	-660	100
KIA 905	355.5	18520	125	6a	760	*21941*	_27.8						
	360.5	——		6a/b	760	*22080*	77.3	UCI 191626	358.5	18760	350	240	520
KIA 41675	361.0	**18730**	130	6b	580	*22087*	_13						
KIA 41678	361.5	**18620**	110	6b	580	*22100*							
KIA 906	377.5	18730	125	6b base	580	*22300*		AWI 1266.1.1	377	18,875	25	145	435
KIA 907	399.5	19230	140										
KIA 908	412.5	19670	150										
KIA 909	422.5	19940	140										

BOLD = mean of double dates

BOLD = plateau boundaries

AMS ^{14}C ages of planktic and benthic samples were measured at the Leibniz Laboratory, University of Kiel (KIA numbers), the AWI AMS facility in Bremerhaven (AWI numbers), and the Keck Carbon Cycle AMS facility (UCI numbers), University of California, Irvine.

DATA SOUCE: **Planktic 14C ages of**
Voelker, 1999, supplemented by 14C data of
Sarnthein et al., 2015,
(plus conversion to cal. age estimates of IntCal20 after Bronk Ramsey et al., 2020).
Benthic 14C ages: This study

Table 2: Detrital and authigenic data of radiogenic εNd and Pb isotopes in Core PS2644

(see xlsx-Table 2)

==========

Supplementary Text no.1

Derivation of paleoceanographic proxy values

*** Reduced sea surface salinity and meltwater dilution** of local surface and subsurface waters are inferred from strongly reduced planktic $\delta^{18}O$ values of *Neogloboquadrina pachyd erma* sin. (Nps) that in part also serve as tracer of increased sea surface temperature (SST) both below an ongoing sea ice cover in the Icelandic Sea and in the eastern Nordic Seas (Voelker, 1999; van Kreveld et al., 2000; Sarnthein et al., 2001; Simstich et al., 2003; Sadatzki et al., 2020).

* **Straight estimates of SST** are derived from census counts of planktic foraminiferal species (Pflaumann et al., 2003; Sarnthein et al., 2001; Voelker, 1999).

* **The particular minimum of bottom water temperature** (BWT) at Site PS2644 has been deduced from maximum epibenthic $\delta^{18}O$ values measured on single specimens of epibenthic *Cibicides lobatulus* and *C. wuellerstorfi* (suppl. by 0.64 interpretation of this record is complex, since each sediment sample is providing a 1–2 and/or interannual temperature oscillations, if we assume a widely constant bottom water salinity. For the interval 22–18.4 cal. ka, however, the maximum value of each $\delta^{18}O$ array is strictly confined to 5.6 18.4–15.1 cal. ka, where maximum $\delta^{18}O$ values are confined to 4.8 to constrain a short-term major shift in minimum bottom water temperature corresponding to ˜3.4°C (following the conversion of $\delta^{18}O$ values by Shackleton, 1974; Ganssen, 1983).

* **Short-term oscillations of BWT** were also derived from Mg/Ca ratios of *C. neoteretis* at neighbor Site GS15-198-36CC for stadials GS4 to GS9 and interstadials GI5-GI8 during MIS3 (Sessford et al., 2018). The latter temperature record forms a valuable analog to identify potential differential bottom water sources assumed for the interstadial scenario of late LGM and the onset and culmination of stadial HS1.

* **Different levels of bottom water ventilation** and their seasonal and/or interannual variability at PS2644 are traced by means of epibenthic $\delta^{13}C$ values of single specimens of epibenthic *C. lobatulus* (Fig. 4). Analytical details of measuring stable C and C isotope data of single specimens are given in Voelker (1999*).*

* **Spatial and temporal MRA variations of subsurface waters**(Table 1) are deduced by means of ^{14}C plateau tuning outlined in the main text and presented in ^{14}C yr (details in Sarnthein et al., 2020). Low MRA serve as tracer of open, high MRA as tracer of impeded CO_2 exchange surface waters with the

atmosphere. At Site PS2644 the exchange was blocked by long-term predominant sea ice cover (per analogy to MIS3; Sadatzki et al., 2020) and by Arctic sourced waters of the EGC (Fig. 2a). Likewise, MRA at Site GIK23074 are temporarily very high (˜2000 yr and more), hence also suggesting a lid of Arctic sourced surface waters (Fig. 2b).

* **(Raw, i.e., uncorrected) estimates of ventilation ages of bottom waters** (Table 1) record their last contact with the atmosphere and form a robust tracer of deep-water masses since their last contact with the atmosphere (Matsumoto, 2007). The short-term age variations are simply deduced from the age difference between paired epibenthic and planktic ^{14}C ages in addition to the paired planktic MRA (following rules defined by Cook and Keigwin, 2015, and Sarnthein et al., 2020). Temporal and spatial differences in benthic ventilation age serve as tracer of a differential origin of bottom waters either in the Nordic Seas and/or the North Atlantic. Brine water-derived bottom waters are earmarked by the close affinity of their ventilation age to paired high planktic MRA and by 'aberrant' light benthic δ^{18}O values that closely reflect the δ^{18}O level of nearby of surface waters freezing during late summer (Bauch and Bauch, 2001).

* **The geometry of past bottom water circulation** is further constrained by authigenic and detrital Nd and Pb isotopes at Site PS2644. We use both isotope systems together in order to constrain the provenance of sediment and deep-water currents. However, it is well established that the authigenic sediment fraction in regions of volcanic input can be overprinted in situ by detrital contributions of radiogenic Nd; accordingly, the authigenic Nd isotope data must be interpreted with caution (Elmore et al., 2011, Blaser et al., 2016). We thus largely constrain out interpretations on the radiogenic isotope data of the detrital sediment fraction (see also Struve et al., 2019).

Nd and Pb isotope data were analysed from the same solutions. Sediments were leached with a weak acid-reductive solution as described by Blaser et al. (2020) and Blaser et al. (2016). Afterwards the remaining sediment was digested with an automated micro wave system employing a mixture of HNO_3 and HBF_4 under high pressure and temperature. The sample solutions were purified with established column chromatography methods (Blaser et al. (2016), Gutjahr et al. (2007)) and their isotopic ratios measured with a Neptune Plus MC-ICP-MS at the University of Lausanne.

For Nd isotopes, instrument-induced mass fractionation was corrected to a ^{146}Nd/^{144}Nd value of 0.7219. The corrected ^{143}Nd/^{144}Nd ratios were then normalised to the accepted value of 0.512115 based on repeatedly measured JNdi-1 standard solutions (Tanaka et al., 2000). Nd isotope signatures are reported as εNd = ([(^{143}Nd/^{144}Nd)$_{\text{sample}}$/ (^{143}Nd/^{144}Nd)$_{\text{CHUR}}$] - 1) * 10,000, where (^{143}Nd/^{144} Nd)$_{\text{CHUR}}$ = 0.512638 (Jacobsen and Wasserburg, 1980). The reproducibility was determined via in-house standard solutions to be 0.3 εNd units (2 standard deviations).

Pb isotopes were measured with a Tl-doping technique for exponential mass bias correction and all three isotopic ratios were normalised to SRM NBS 981 (Gutjahr et al., 2007, Galer and Abouchami, 1998). Reproducibilities of ^{206}Pb/^{204}Pb varied between 0.3 and 4.3 * 10^{-3}, which is far smaller than the variation observed in sediments of Site PS2644 or the regional end members.

==========

REFERENCES

Andrews, J.T., Voelker, A.H.L. 2018: "Heinrich events" (& sediments): A history of terminology and recommendations for future usage. *Quaternary Science Reviews* 187, 31-40.

Ausin, B., Sarnthein, M., Haghipour, N., 2021. Glacial-to-deglacial reservoir and ventilation ages on the southwest Iberian continental margin. *Quaternary Science Reviews* , 255, 106818 (1-12 pp.),

Balmer, S., Sarnthein, M. 2018: Glacial-to deglacial changes in North Atlantic meltwater advection and deep-water formation – Centennial-to-millennial-scale ^{14}C records from the Azores Plateau. *Geochimica Cosmochimica Acta* , 236, 399-415, https://doi.org/10.1016/j.gca.2018.03.001.

Bauch, D., Bauch, H. 2001: Last glacial benthic foraminiferal $\delta^{18}O$ anomalies in the polar North Atlantic: A modern analogue evaluation. *Journal of Geophysical Research* 106 (C5), 9135-9143.

Biastoch, A., Kaese, R.H., Stammer, D.B. 2003: The sensitivity of the Greenland-Scotland Ridge Overflow to forcing changes. *Journal of Physical Oceanography* 33, 2307-2319.

Biastoch, A., Schwarzkopf, F.U., Getzlaff, K., Rühs, S., Martin, T., Scheinert, M. Schulzki, T., Handmann, P., Hummels, R., Böning, W.C. 2021: Regional imprints of changes in the Atlantic Meridional Overturning Circulation in the eddy-rich ocean model VIKING20X. *Ocean Science* 17, 1177-1211.

Birks, H.H., Gulliksen, S., Haflidason, H., Mangerud, J., Possnert, G. 1996: New radiocarbon dates for the Vedde Ash and Saksunavatn Ash from western Norway. *Quaternary Research* 45, 119-127.

Blaser, P., Gutjahr, M., Pöppelmeier, F., Frank, M., Kaboth-Bahr, S., Lippold, J. 2020: Labrador Sea bottom water provenance and REE exchange during the past 35,000 years. *Earth and Planetary Science Letters*542, 116299, 1-12.

Blaser, P., Lippold, J., Gutjahr, M., Frank, N., Link, J.M., Frank, M., 2016. Extracting foraminiferal seawater Nd isotope signatures from bulk deep-sea sediment by chemical leaching. *Chemical Geology* 439, 189–204. https://doi.org/10.1016/j.chemgeo.2016.06.024

Bollhoffer, A., Eisenhauer, A., Frank, N., Pech, D., Mangini, A. 1996: Thorium and uranium isotopes in a manganese nodule from the Peru basin determined by alpha spectrometry and thermal ionization mass spectrometry (TIMS): Are manganese supply and growth related? *Geologische Rundschau* 85, 577-585.

Brakstad, A, Gebbie, G., Våge, K., Jeansson, E., Olafsdottir S.R. 2023: Formation and pathways of dense water in the Nordic Seas based on a regional inversion. *Progress in Oceanography* 212, 102.981. doi.org/10.21335/NMDC-1271328906,

Bronk Ramsey, C., Heaton, T.J., Schlolaut, G., Staff, R.A., Bryant, C.L., Lamb, H.F., Marshall, M.H., Nakagawa, T. 2020: Reanalysis of the atmospheric radiocarbon calibration record from Lake Suigetsu, Japan. *Radiocarbon* , doi.org/10.1017/RDC2020/18.

Caesar, L., Rahmstorf, S., Robinson, A., Feulner, G., Saba, V., 2018: Observed fingerprint of a weakening Atlantic Ocean overturning circulation. *Nature* 556, 191-196.

Cook M.S. and Keigwin L.D. 2015: Radiocarbon profiles of the NW Pacific from the LGM and deglaciation: Evaluating ventilation metrics and the effect of uncertain surface reservoir ages. *Paleoceanography* 30, 174–195.

Crocker, A.J., Chalk, T.B., Bailey, I., Spencer, M.R., Gutjahr, M., Foster, G.L., Wilson, P.A., 2016. Geochemical response of the mid-depth Northeast Atlantic Ocean to freshwater input during Heinrich events 1 to 4. *Quaternary Science Reviews* 151, 236–254. https://doi.org/10.1016/j.quascirev.2016.08.035

Crocket, K.C., Vance, D., Foster, G.L., Richards, D.A., Tranter, M., 2012. Continental weathering fluxes during the last glacial/interglacial cycle: insights from the marine sedimentary Pb isotope record at Orphan Knoll, NW Atlantic. *Quaternary Science Reviews* 38, 89–99. https://doi.org/10.1016/j.quascirev.2012.02.004

Ditlevsen, P. and Ditlevsen, S., 2023: Warning of forthcoming collapse of the Atlantic meridional overturning circulation. *Nature communications* 14, article no. 4254.

Dreger, D. 2000: Decadal-to-centennial-scale sediment records of ice advance on the Barents shelf and meltwater discharge into the north-eastern Norwegian Sea over the last 40 kyr, *D.Sc. Thesis, Univ. of Ki* el, Kiel, pp. 1–79.

Duplessy, J.-C., Labeyrie, L., Waelbroeck, C. 2002: Constraints on the ocean oxygen isotopic enrichment between the Last Glacial Maximum and the Holocene: Paleoceanographic implications. *Quaternary Science Reviews* 21, 315/330

Eisenhauer, A., Meyer, H., Rachold, V., Tutken, T., Wiegand, B., Hansen, B.T., Spielhagen, R.F., Lindemann, F., Kassens, H., 1999. Grain size separation and sediment mixing in Arctic Ocean sediments: evidence from the strontium isotope systematic. *Chemical Geology* 158, 173–188. https://doi.org/10.1016/S0009-2541(99)00026-1

Elmore, A.C., Piotrowski, A.M., Wright, J.D., Scrivner, A.E., 2011. Testing the extraction of past seawater Nd isotopic composition from North Atlantic deep-sea sediments and foraminifera. *Geochemistry, Geophysics, Geosystems* 12. https://doi.org/10.1029/2011GC003741

Fagel, N., Innocent, C., Gariepy, C., Hillaire-Marcel, C., 2002. Sources of Labrador Sea sediments since the last glacial maximum inferred from Nd-Pb isotopes. Geochimica et Cosmochimica Acta 66, 2569–2581.

Farmer, G.L., Barber, D., Andrews, J., 2003. Provenance of Late Quaternary ice-proximal sediments in the North Atlantic: Nd, Sr and Pb isotopic evidence. Earth and Planetary Science Letters 209, 227–243. https://doi.org/10.1016/S0012-821X(03)00068-2

Galer, S.J.G., Abouchami, W., 1998. Practical application of lead triple spiking for correction of instrumental mass discrimination. Mineralogical Magazine 62 A, 491–492.

Ganssen, G. 1983: Dokumentation von küstennahem Auftrieb anhand stabiler Isotope in rezenten Foraminiferen vor Nordwest Afrika,*Meteor-Forschungsergebnisse* C37, 1–46.

Grootes, P.M., Stuiver, M. 1997:$^{18}O/^{16}O$ variability in snow and ice with 10^{-3} to 10^{-5} year time resolution. *Journal of Geophysical Research* 102 (C12), 26,455-26,470.

Hagen, S. and Hald, M. 2002. Variation in surface and deep-water circulation in the Denmark Strait, North Atlantic, during marine isotope stages 3 and 2. *Paleoceanography* 17 (4):13-1 – 13-16.

Haine, T.W.N. 2021. A conceptual model of polar overturning circulations. *J. Physical Oceanography* 51, 727-744.

Haley, B.A., Frank, M., Spielhagen, R.F., Fietzke, J., 2008. Radiogenic isotope record of Arctic Ocean circulation and weathering inputs of the past 15 million years. *Paleoceanography* 23. https://doi.org/10.1029/2007PA001486

Hanebuth, T. J. J., Stattegger, K., Bojanowski, A., 2009: Termination of the Last Glacial Maximum sea-level low-stand: The Sunda-Shelf data revisited. *Global and Planetary Change* 66, 76-84.

Hansen, B., Østerhus, S. 2000: North Atlantic-Nordic Seas exchange.*Progress Oceanography* 45, 109-208, doi.org/10.1016/S0079-6611(99)00052-X

Hodell, D.A., Nicholl, J.A., Bontognali, T.R.R., plus 9 coauthors 2017: Anatomy of Heinrich Layer 1 and its role in the last deglaciation.*Paleoceanography* 32, 284-303, doi:10.1002/2016PA00302.

Hubberten, H.-W. (edit.) 1995: Die Expedition Arktis-X2 mit FS "Polarstern" in 1994. *Berichte zur Polarforschung* 174: 186 pp.

Ivy-Ochs, S. (2015): Glacier variations in the European Alps at the end of the last glaciation. – *Cuadernos de Investigación Geográfica* , 41: 295–315.

Jacobsen, S.B., Wasserburg, G.J., 1980. Sm-Nd isotopic evolution of chondrites. *Earth and Planetary Science Letters* 50, 139–155.

Jansen, E., Hesselberg Christensen, J., Dokken, T., et al., 2020: Past perspectives on the present era of abrupt Arctic climate change.*Nature Climate Change* 10, 714-721.

doi.org/101038/s41558-020-0860-7.

Kaese, R.H., Oschlies, A. 2000: Flow through Denmark Strait. *J. Geophysical Research* 105 (28):527,528,546.

Kaese, R.H., Girton, J.B., Sanford, T.B. 2003: Structure and variability of the Denmark Strait Overflow: Model and observations. *J. Geophysical Research, Oceans* 108 (C6).

https://doi.org/10.1029/2002JC001548

Kempton, P.D., Fitton, J.G., Saunders, A.D., Nowell, G.M., Taylor, R.N., Hardarson, B.S., Pearson, G., 2000. The Iceland plume in space and time: a Sr–Nd–Pb–Hf study of the North Atlantic rifted margin. *Earth and Planetary Science Letters* 177, 255–271. https://doi.org/10.1016/S0012-821X(00)00047-9

Kösters, F. 2004. Denmark Strait overflow: comparing model results and hydraulic transport estimates. *J. Geophysical Research*109:C10011, DOI 10.1029/2004JC002297

Kösters, F., Käse, R.H., Schmittner, A., Herrmann, P. 2005: The effect of Denmark Strait overflow on the Atlantic Meridional Overturning Circulation. *Geophysical Research Letters* 32, L04602, doi:10.1029/2004GL022112.

Kuijpers, A., Troelstra, S.R., Prins, M.A., et al. 2003: Late Quaternary sedimentary processes and ocean circulation changes at the southeast Greenland margin. *Marine Geology* 195: 109-129,

Kutschera, W., Müller, W. 2003: "Isotope language" of the Alpine Iceman investigated with AMS and MS. *Nuclear Instruments and Methods in Physics Research* B204, 705-719.

Labeyrie, L. D., Duplessy, J.C., Blanc, P.L. 1987: Variations in mode of formation and temperature of oceanic deep waters over the past 125,000 years, *Nature* 327, 477–482.

Larkin, C.S., M. M. Ezat, R. Spielhagen, H. Bauch, R. Noormets, L. Polyak, S. Moreton, N.L. Roberts, T. L. Rasmussen, M. Sarnthein, E. T. Tipper, A. M. Piotrowski, 2022. Resolving Nordic Seas deep-water formation during the last glacial maximum. – *Nature geoscience* , 15, 1-7. doi.org/10.1038/s41561-022-01050-w

Lomitschka, M., Mangini, A. 1999: Precise Th/U-dating of small and heavily coated samples of deep-sea corals, *Earth and Planetary Science Letters* 170, 391-401.

Macrander, A., Käse, R.H., Send, U., Valdimarsson, H., Jónsson, S., 2007: Spatial and temporal structure of the Denmark Strait Overflow revealed by acoustic observations. *Ocean Dynamics* 57:75-89.

Magana, A.L., Southon, J.R., Kennett, J.P., Brendan Roark E., Sarnthein, M., Stott, L.D. 2010: Resolving the cause of large differences between deglacial benthic fauna radiocarbon measurements in the Santa Barbara Basin. *Paleoceanography* , 25, PA4102.doi:10.1029/2010PA002011,2010.

Matsumoto, K. 2007: Radiocarbon-based circulation age of the world oceans, *J. Geophysical Research: Oceans* 112(C9), C09004. https://doi.org/10.1029/2007JC004095.

Meland, M.Y., Dokken, T.M., Jansen, E., Hevrøy, K., 2008. Water mass properties and exchange between the Nordic seas and the northern North Atlantic during the period 23–6 ka: Benthic oxygen isotopic evidence.*Paleoceanography* 23, doi: 10.1029/2007PA001416.

Millo, C., Ms. Sarnthein, H. Erlenkeuser, 2006: Variability of the Denmark Strait Overflow during the Last Glacial Maximum. *Boreas,*35, 50-60.

Mix, A.C., Bard, E. and Schneider, R. 2001: Environmental processes of the Ice age: Land, oceans, glaciers (EPILOG), *Quaternary Science Rev* iews 20, 627-658.

Neff, U., Bollhoffer, A., Frank, A., Mangini, A. 1999: Explaining discrepant depth profiles of 234U/238U and $230Th_{exec}$ in Mn-crusts, *Geochemica et Cosmochimica Ac* ta.

Peate, D.W., Stecher, O. 2003. Pb isotope evidence for contributions from different Iceland mantle components to Palaeogene East Greenland flood basalts. *Lithos* 67, 39–52. doi.org/10.1016/S0024-4937(02)00250-5

Pflaumann, U., Sarnthein, M., Chapman, M., d'Abreu, L., plus 10 coauthors 2003: Glacial North Atlantic: Sea-surface conditions reconstructed by GLAMAP 2000. *Paleoceanography* 18 (3), 1065.

doi:10.1029/2002PA000774

Sadatzki, H., Maffezzoli, N., Dokken, T.M., plus 9 coauthors 2020: Rapid reductions and millennial-scale variability in Nordic Seas' sea ice cover during abrupt glacial climate changes. *PNAS* 117 (47), 29478-29486.

Sarnthein, M., Winn, K., Jung, S.J., Duplessy, J.C., Labeyrie, L., Erlenkeuser, H., Ganssen, G. 1994: Changes in east Atlantic deep-water circulation over the last 30,000 years: Eight time slice reconstructions. *Paleoceanography* 9(2), 209–267.

Sarnthein, M., K. Stattegger, D. Dreger, H. Erlenkeuser, P. Grootes, B. Haupt, S. Jung, T. Kiefer, W. Kuhnt, U. Pflaumann, C. Schäfer-Neth, H. Schulz, M. Schulz, D. Seidov, J. Simstich, S. van Kreveld-Alfane, E. Vogelsang, A. Völker, M. Weinelt, 2001: Fundamental modes and abrupt changes in North Atlantic circulation and climate over the last 60 ky - Concepts, reconstruction, and numerical modelling. - In: P. Schäfer et al. (eds): *The northern North Atlantic: A changing environment*(Springer Verlag) 365-410.

Sarnthein, M., Balmer, S., Grootes, P.M., Mudelsee, M. 2015: Planktic and benthic ^{14}C reservoir ages for three ocean basins, calibrated by a suite of ^{14}C plateaus in the glacial-to-deglacial Suigetsu atmospheric ^{14}C record.*Radiocarbon* 57, 129-151.

Sarnthein, M., Küssner, K., Grootes, P.M., Ausin, B., Eglinton, T., Muglia, J., Muscheler, R., Schlolaut, G. 2020. Plateaus and jumps in the atmospheric radiocarbon record – Potential origin and value as global age markers for glacial-to-deglacial paleoceanography, a synthesis.*Climate of the Past* 16, 2547–2571. URL: doi: 10.5194/cp-16-2547-2020.

Sarnthein, M., Grootes, P.M., Mudelsee, M. 2023. Centennial to millennial-sale fluctuations of the Lake Suigetsu atmopsheric^{14}C record represent real ^{14}C features over last glacial-to-deglacial times. *Radiocarbon* 65 (4), DOI:10.1017/RDC.2023.47.

Schlitzer, R. 2002: Interactive analysis and visualization of geoscience data

with Ocean Data View, *Comput. Geoscience* 28, 1211-1218.

Sessford, E.G., Tisserand, A.A., Risebrobakken, B., Andersson. C., Dokken, T., and Jansen E. 2018: High-resolution benthic Mg/Ca temperature record of the intermediate water in the Denmark Strait across D-O stadial-interstadial cycles. *Paleoceanography and Paleoclimatology* 33, 1169-1185. doi.org/10.1029/2018PA003370

Sessford, E.G., Jensen, M.F., Tisserand, A.A., Muschitiello, F., Dokken, T., Nisancioglu, K.H., and Jansen, E., 2019: Consistent fluctuations on intermediate water temperature off the coast off Greenland and Norway during Dansgaard-Oeschger events, *Quaternary Science Reviews* 223, 105887, 1-17.

Shackleton, N.J., 1974: Attainment of isotopic equilibrium between ocean water and the benthonic foraminifera genus *Uvigerina* : Isotopic change in the ocean during the last Glacial, *Colloques Internationaux du C.N.R.S* . 219: 203-209.

Siedler, G., Church, J., Gould, J. (eds.) 2001: *Ocean circulation and climate. Observing and modelling the global ocean.* Academic Press San Diego - New York, 1-715.

Simon, M.H., Rutledal, S., Menviel, L., Zolles, T., Haflidason, H., Born, A., Berben, S.M., Dokken, T.M. 2023: Atlantic inflow and low sea-ice cover in the Nordic Seas promotes Fennoscandian Ice Sheet growth during the Last Glacial Maximum. *Communications Earth and Environment* 4, 385, doi.org/10.1038/s43247-0223-01032-9.

Struve, T., Roberts, N.L., Frank, M., Piotrowski, A.M., Spielhagen, R.F., Gutjahr, M., Teschner, C., Bauch, H.A. 2019: Ice-sheet-driven weathering input and water mass mixing in the Nordic Seas during the last 25,000 years. *Earth and Planetary Science Letters* 514, 108-118.

Svensson, A., Andersen, K.K., Bigler, M., Clausen, H.B., Dahl-Jensen, D., Davies, S.M., Johnsen, S.J., Muscheler, R., Parrenin, F., Rasmussen, S.O., Röthlisberger, R., Seierstad, I., Steffensen, J.P., and Vinther,

B.M. 2008: A 60,000-year Greenland stratigraphic ice core chronology,*Climate of the Past* 4, 47–57.

Tanaka, T., Togashi, S., Kamioka, H., Amakawa, H., Kagami, H., Hamamoto, T., Yuhara, M., Orihashi, Y., Yoneda, S., Shimizu, H., Kunimaru, T., Takahashi, K., Yanagi, T., Nakano, T., Fujimaki, H., Shinjo, R., Asahara, Y., Tanimizu, M., Dragusanu, C., 2000. JNdi-1: a neodymium isotopic reference in consistency with LaJolla neodymium. Chemical Geology 168, 279–281. https://doi.org/10.1016/S0009-2541(00)00198-4

Thornalley, D.J.R., Barker, S., Broecker, W.S., Elderfield, H. and McCave, I.N. 2011. The deglacial evolution of the North Atlantic deep convection. *Science* **331** , 202-205.

Våge, K., Pickart, R.S., Spall, M.A., et al. s2011: Significant role of the North Iceland Jet in the formation of Denmark Strait overflow water.*Nature geoscience* 4, *DOI: 10.1038/NGEO1234*

Van Kreveld, S., M. Sarnthein, H. Erlenkeuser, P. Grootes, S. Jung, M.J. Nadeau, U. Pflaumann, and A. Voelker, 2000: Potential links between surging ice sheets, circulation changes, and the Dansgaard-Oeschger cycles in the Irminger Sea. *Paleoceanography* 15: 425-442.

Voelker, A. 1999: Dansgaard-Oeschger events in ultra-high resolution sediment records from the Nordic Seas. *Berichte-Reports Institut für Geowissenschaften* , University of Kiel, 9, pp. 1-278.

Voelker, A.H.L., P.M. Grootes, M.J. Nadeau, & M. Sarnthein, 2000: 14C levels in the Iceland Sea from 25-53 kyr and their link to the Earth's magnetic field intensity. - *Radiocarbon* 42 (3):437-452.

Voelker, A.H.L., Haflidason, H., 2015: Refining the Icelandic tephrachronology of the last glacial period – The deep-sea core PS2644 record from the southern Greenland Sea. *Global and Planetary Change* 131, 32-62.

Voelker, A., M. Sarnthein, P.M. Grootes, H. Erlenkeuser, C. Laj, A. Mazaud, M. Nadeau, and M. Schleicher, 1998: Correlation of marine 14C ages from the Nordic Seas with the GISP2 Isotope record: Implications for radiocarbon calibration beyond 25 kyr. *Radiocarbon* 40, 517-534.

Waelbroeck, C., Skinner, L.C., Labeyrie, L., Duplessy, J.-C., Michel, E., Riveiros, N.V., Gherardi, J.-M., and Dewilde, F. 2011: The timing of deglacial circulation changes in the Atlantic. *Paleoceanography*26, PA3213, https://doi.org/10.1029/2010PA002007.

Weinelt, M., Sarnthein, M., Vogelsang, E., and Erlenkeuser, H. 1991: Early decay of the Barents Shelf ice shelf – Spread of stable isotope signals across the eastern Norwegian Sea. *Norsk Geologisk Tidsskift* 71, 137-140.

Weinelt, M., Vogelsang, E., Kucera, M., Pflaumann, U., Sarnthein, M., Voelker, A., Erlenkeuser, H., Malmgren, B.A. 2003: Variability of North Atlantic heat transfer during MIS 2. *Paleoceanograph* y 18, 1-16, doi:10.1029/2002PA000772

Whitehead, J. A., Leetmaa, A., Knox, R. A. 1974: Rotating hydraulics of strait and sill flows. *Geophysical Fluid Dynamics* 6, 101–125.

Wolff, E.W., Chappelaz, J., Blunier,T., Rasmussen, S.O., Svensson, A. 2010: Millennial-scale variability during the last glacial: The ice core record. *Quaternary Science Reviews* 29, 2828-2838.

doi.org/10.1016/j.quascirev.2009.10.013

You, D., Stein, R., Fahl, K., Williams, M.C., Schmidt, D.N., McCave, I.N., Barker, S., Schefuß, Niu, L., Kuhn, G., Niessen, F. 2023: Last deglacial abrupt climate changes caused by meltwater pulses in the Labrador Sea. *Communications Earth & Environment* 4:81.

doi.org/10.1038/s43247-023-00743-3